

Likelihood-based Inference for Partially Observed Epidemics on Dynamic Networks

Fan Bu¹, Allison E. Aiello², Jason Xu^{*§1}, and Alexander Volfovsky^{*1}

¹Department of Statistical Science, Duke University

²Gillings School of Global Public Health, University of North Carolina at Chapel Hill[†]

Abstract

We propose a generative model and an inference scheme for epidemic processes on dynamic, adaptive contact networks. Network evolution is formulated as a link-Markovian process, which is then coupled to an individual-level stochastic SIR model, in order to describe the interplay between the dynamics of the disease spread and the contact network underlying the epidemic. A Markov chain Monte Carlo framework is developed for likelihood-based inference from partial epidemic observations, with a novel data augmentation algorithm specifically designed to deal with missing individual recovery times under the dynamic network setting. Through a series of simulation experiments, we demonstrate the validity and flexibility of the model as well as the efficacy and efficiency of the data augmentation inference scheme. The model is also applied to a recent real-world dataset on influenza-like-illness transmission with high-resolution social contact tracking records.

Keywords: stochastic susceptible-infectious-recovered (SIR) model, continuous-time Markov chains, Bayesian data augmentation, conditional simulation, mobile healthcare, network inference.

*Joint last authors. [§]Corresponding author: jason.q.xu@duke.edu

[†]The eXFLU data were supported by U01 CK000185, AV and AA were partially supported by R01 EB025021, AV and FB were partially supported by W911NF1810233, JX was partially supported by DMS 1606177.

1 Introduction

The vast majority of epidemiological models, such as the well-known susceptible-infectious-recovered (SIR) model, rely on compartmentalizing individuals according to their disease status (Kermack and McKendrick, 1927). Classically, such models describe population-level behavior under a “random mixing” assumption that an infectious individual can spread the disease homogeneously to any susceptible individual (Kermack and McKendrick, 1927; Bailey et al., 1975; Anderson and May, 1992). In the last two decades, an alternative assumption—that the disease is transmitted through links in a contact network—has gradually gained popularity. It has been found that the contact network structure can fundamentally impact the behavior of epidemic processes (Wallinga et al., 1999; Edmunds et al., 1997, 2006; Mossong et al., 2008; Volz and Meyers, 2008; Melegaro et al., 2011); on the other hand, the network structure can in turn be influenced by disease status of individuals as well (Bell et al., 2006; Funk et al., 2010; Eames et al., 2010; Van Kerckhove et al., 2013).

This growing interest—alongside technological advances in mobile data—has spurred efforts on collecting high-resolution data that inform the dynamics of the contact network (Vanhems et al., 2013; Barrat et al., 2014; Voirin et al., 2015; Kiti et al., 2016; Aiello et al., 2016; Ozella et al., 2018). Data of this type has most recently been collected by Ministry Of Health, State of Israel (2020) and Korea Centers for Disease Control & Prevention (2020). However, there is a gap between the demand to analyze such emergent data and available methods: a recent review by Britton (2020) outlines possible approaches to inference for epidemic models on networks and calls to attention considerable challenges—in particular, key terms such as transition probabilities that appear in central quantities such as likelihood expressions are unavailable. Accounting for the relationship between disease spread and the underlying contact network during inference is crucial to accurately estimating parameters describing the inherent properties of the disease, and moreover has direct practical implications on epidemic control and intervention. Policies such as quarantine or suppression are naturally described as changes to the contact network, and yet modeling approaches are largely restricted to prospective simulations and/or analysis based on static networks in lieu of direct inference from modern data. Recent examples can be seen in analyses for

COVID-19 (Ferguson et al., 2020) and for MERS-CoV transmissions (Yang and Jung, 2020).

To address this methodological gap, we develop a statistical model that describes the mutual interplay between SIR-type epidemics and an underlying dynamic network, together with a tractable inferential framework to fit such models to modern time-resolved datasets. In particular, we propose a stochastic generative model that can be fit to data using likelihood-based methods. We present a Bayesian data augmentation scheme that accommodates partial observations such as missing recovery times that are common in real data while quantifying uncertainty in estimated parameters.

The majority of existing work on epidemic processes over networks adopt a deterministic approach based on ordinary differential equations (ODEs) models (Kiss et al., 2012; Ogura and Preciado, 2017; Van Segbroeck et al., 2010; Tunc et al., 2013; WHO Group, 2006; Volz and Meyers, 2007; Shaw and Schwartz, 2008; Volz, 2008). Such approaches do not provide a measure of uncertainty, and do not offer probabilistic interpretations. Our framework builds upon previous stochastic (and likelihood-based) methods that either do not consider network dynamics (Britton and O’Neill, 2002; Dong et al., 2012; Fan et al., 2015, 2016), or do not model the contact network at all (Cauchemez et al., 2006; Hoti et al., 2009; Britton, 2010; Fintzi et al., 2017; Ho et al., 2018). Moreover, the proposed inference scheme accommodates partially observed data, with a focus on unknown recovery times in this paper. Handling missing data even **without** network constraints is already challenging, and often requires simplifying assumptions (Cauchemez and Ferguson, 2008) or computationally intensive simulation-based inference (He et al., 2010; Andrieu et al., 2010; Pooley et al., 2015).

The rest of the paper is organized as follows: Section 2 reviews background on epidemic models (focusing on the stochastic SIR model) and dynamic network processes. Section 3 formulates the generative model and derives maximum likelihood estimators as well as Bayesian posterior distributions based on the complete data likelihood. Section 4 describes a Bayesian inference scheme that deals with incomplete observations on individual recovery times. Section 5 and 6 present experiment results on simulated datasets and a real-world dataset. Finally Section 7 provides further discussions.

2 Background

Compartmental Epidemiological Models Compartmental models divide individuals into non-overlapping subsets according to their disease statuses. In classical models, the change in these subpopulations over time are described by ordinary differential equations (ODEs) (Hethcote, 2000). One widely used model is the susceptible-infectious-recovered (SIR) model, which assumes three disease statuses—susceptible (S), infectious (I), and recovered (or removed, R). On a closed population of N individuals (with N sufficiently large), the dynamics of the deterministic SIR model can be expressed as

$$\frac{dS(t)}{dt} = -\beta S(t)I(t), \quad \frac{dI(t)}{dt} = \beta S(t)I(t) - \gamma I(t), \quad (1)$$

where $S(t)$ and $I(t)$ refer to the number of susceptible and infectious individuals at time t , respectively, and the number of recovered individuals satisfies $R(t) = N - [S(t) + I(t)]$. The parameters describe the epidemic mechanistically: here β is interpreted as the rate of disease transmission **per contact between** an S individual and an I individual, and γ is the rate of recovery for an I individual.

By setting the growth rate of infection to be proportional to $S(t)I(t)$, the model in (1) implicitly assumes that any two members can interact with each other. This assumption is easily violated in reality, where an individual only maintains contact with a limited number of others. Moreover, the differential equations can only account for the average, expected behavior of the process, but the transmission of an infectious disease exhibits randomness and uncertainty by nature.

To account for the underlying network structure of a population as well as the random nature of an epidemic process, we adopt an **individual-level, stochastic** variation of the SIR model, similar to that used in Auranen et al. (2000). An individual of status S (susceptible) at time t (> 0) changes disease status to I (infectious) at time $t + h$ (h is an infinitesimal quantity) with a probability that is dependent on both the infection rate β **and** his/her contacts at time t . An infectious individual at time t becomes a member of the R (recovered) sub-population at time $t + h$ with a probability determined by the recovery rate γ . Specifically, for any susceptible individual p_1 and infectious individual p_2 in the population

at t , conditioned on the current overall state of the process, \mathcal{Z}_t , then

$$Pr(p_1 \text{ gets infected by } p_2 \text{ at } t + h \mid \mathcal{Z}_t) = \beta h + o(h) \quad (2)$$

if p_1 and p_2 are in contact at t , and

$$Pr(p_2 \text{ recovers at } t + h \mid \mathcal{Z}_t) = \gamma h + o(h). \quad (3)$$

Basic Network Concepts A network, or a graph, is a two-component set, $\mathcal{G} = \{\mathcal{V}, \mathcal{E}\}$, where \mathcal{V} is the set of N nodes and \mathcal{E} is the set of links. A network can be represented by its “adjacency matrix”, \mathbf{A} , where $\mathbf{A}_{ij} = 1$ indicates there is a link from node i to j . Since most infectious diseases can be transmitted in both directions through a contact, we assume that the adjacency matrix is **symmetric**, $\mathbf{A}_{ij} = \mathbf{A}_{ji}$.

A special network structure is the fully connected network (or the complete graph), \mathcal{K}_N , and its adjacency matrix \mathbf{A} satisfies $\mathbf{A}_{ij} = 1$ for any $i \neq j$. This network structure corresponds to the widely adopted “random mixing” assumption in epidemiological models, which, as stated before, may be restrictive and unrealistic. Therefore, in the rest of the paper, we instead consider **arbitrary** network structures underlying the population.

Temporal and Adaptive Networks Interactions between individuals are dynamic in nature, and such dynamics is important when modeling epidemic processes (Masuda and Holme (2017); also as demonstrated later in Section 5.1). We consider a continuous-time link-Markovian model for temporal networks (Clementi et al., 2010; Ogura and Preciado, 2016). Following the symmetric network assumption stated above, for two individuals i and j ($i < j$) who are not in contact at time t , they form a link at time $t + h$ ($h \ll 1$) with probability αh , where α is the link activation rate. Similarly, if there is an edge between i and j at time t , then the edge is deleted at time $t + h$ with probability ωh , where ω is some link termination rate.

If, instead, individuals establish and dissolve their social links with rates that vary according to their disease statuses, then the evolution of the network is coupled to the epidemic process and thus becomes **adaptive**. This mechanism can be described via instantaneous rates of single-link changes. For any two individuals i and j , their corresponding entry in

the adjacency matrix is modeled as a $\{0, 1\}$ -valued Markov process, $\mathbf{A}_{ij}(t), t > 0$. Suppose that at time t , i is of status A , j is of status B ,¹ then for an infinitesimal quantity h ,

$$Pr(\mathbf{A}_{ij}(t+h) = \mathbf{A}_{ji}(t+h) = 1 \mid \mathbf{A}_{ij}(t) = 0) = \alpha_{AB}h + o(h); \quad (4)$$

$$Pr(\mathbf{A}_{ij}(t+h) = \mathbf{A}_{ji}(t+h) = 0 \mid \mathbf{A}_{ij}(t) = 1) = \omega_{AB}h + o(h). \quad (5)$$

Here $\alpha_{AB}(= \alpha_{BA})$ is the activation rate for an A - B type link, and similarly, $\omega_{AB}(= \omega_{BA})$ is the termination rate for an A - B type link.

3 Epidemic Processes over Adaptive Networks

3.1 The Generative Model

In this subsection, we lay out a stochastic data generative process (referred to as the “generative model”) for the joint evolution of an individualized SIR process on a networked population and the dynamics of the contact network. In contrast to the ODE literature and existing network models described in Section 1, the key feature of the model is the **interplay** between epidemic progression and network adaptation. On one hand, transmission of infection depends on the existence of susceptible-infectious links, which may change through time; on the other hand, network links temporally update in a manner that in turn depends on individual disease status.

We formulate this complex process as a continuous-time Markov chain that comprises all individual-level events described in Section 2. The joint evolution of the individual Poisson processes described by (2)-(5) can be described via a competing risks construction. By the Markov property, the time until each type of event has an exponential waiting time, and thus the time to next event in the joint process remains exponentially distributed (Guttorp and Minin, 2018). Events occur stochastically and are of one of the four types:

- **Infection:** The disease is transmitted through a link between an S (susceptible) and an I (infectious) individual (S - I link) with rate β ;

¹Here $A, B \in \{S, I, R\}$, and we only consider $i < j$ since the network is assumed symmetric.

- **Recovery:** Each I individual recovers with rate γ independently;
- **Link activation:** A link is formed at rate $\alpha_{AB}(= \alpha_{BA})$ between an individual of status A and another of status B who are not connected, where $A, B \in \{S, I, R\}$;
- **Link termination:** An existing link is removed at rate $\omega_{AB}(= \omega_{BA})$ between an individual of status A and another of status B , where $A, B \in \{S, I, R\}$.

This formulation will allow for joint inference of both disease spread and network evolution. As illustrated in the next subsection, inference is straightforward when all the events are fully observed. Furthermore, this formulation implies a relatively simple generative process at the population level. Conditioned on the current state of the process \mathcal{Z}_t at time $t (> 0)$, the very next event of the entire process is the **earliest** event that occurs among the four competing processes by the superposition property:

- **Infection:** An infection occurs with rate $\beta SI(t)$, where $SI(t)$ is the number of S - I links at time t ;
- **Recovery:** A recovery occurs with rate $\gamma I(t)$, where $I(t)$ is the number of infectious individuals at time t ;
- **Link activation:** An A - B link is established with rate $\alpha_{AB}M_{AB}^d(t)$, where $M_{AB}^d(t)$ is the number of disconnected A - B pairs at time t ;
- **Link termination:** An A - B link is dissolved with rate $\omega_{AB}M_{AB}(t)$, where $M_{AB}(t)$ is the number of connected A - B pairs at time t .

We may interpret this generative model as a generalization of two simpler models. If we set $\alpha_{AB} \equiv \alpha$ and $\omega_{AB} \equiv \omega$ for any status A and B , the coupled process reduces to a **decoupled** process, where network evolution is **independent** of individual disease status. Moreover, if we fix $\alpha \equiv \omega \equiv 0$, the process is further reduces to an SIR process over a **static** network.

Here we assume that the population size N is fixed, and that at $t = 0$, the initial network \mathcal{G}_0 as well as $I(0)$ initial infection cases are observed. We summarize a list of model parameters and notation in Table 1.

Table 1: Table of parameters and notation.

Parameter	Description
β	infection rate
γ	recovery rate
α	link activation rate for a currently disconnected pair
ω	link termination rate for a currently connected pair
α_{AB}	link activation rate for a currently disconnected A-B pair
ω_{AB}	link termination rate for a currently connected A-B pair
Notation	Description
N	total population size (assumed to remain fixed throughout the process)
T_{\max}	maximum observation time
\mathcal{Z}_t	state of the process at time t (including the epidemic status of every individual and the social network structure at time t)
\mathcal{G}_t	social network structure (a graph) at time t
$S(t), I(t)$	numbers of susceptible/infectious individuals in the population at time t
$H(t)$	number of healthy (not infectious) individuals in the population at time t
$I_k(t)$	number of infectious individuals in person k 's neighborhood at time t
$SI(t)$	number of S - I links in the network at time t
$M(t)$	total number of edges in the network at time t
$M_{AB}(t)$	number of A - B links at time t
$M_{AB}^d(t)$	number of disconnected A - B pairs at time t
n_E, n_R	counts of infection events and recovery events in the process
n_N	count of network events in the process (each event is the activation or termination of a single link)
C, D	total counts of link activation/termination
C_{AB}, D_{AB}	counts of link activation/termination events for A - B pairs

3.2 Complete Data Likelihood and Parameter Inference

Derivation of complete data likelihood Suppose n_E infection events and n_R recovery events are observed in total. Let i_k be the infection time for individual k ($k = 1, 2, \dots, n_E$),

r_k be k 's recovery time (if $r_k > T_{\max}$, k 's recovery is not observed), and without loss of generality, set $i_1 = 0$. Recall that the widely used ‘‘random mixing’’ assumption in classical epidemiological models is equivalent to assuming that the contact network is a complete graph, \mathcal{K}_N , and the individual-based complete data likelihood under this assumption is ²

$$\mathcal{L}(\beta, \gamma) = p(\text{epidemic events}|\beta, \gamma) = \gamma^{n_R} \prod_{k=2}^{n_E} [\beta I(i_k)] \exp\left(-\int_0^{T_{\max}} [\beta S(u)I(u) + \gamma I(u)] du\right).$$

To account for the contact network, let \mathcal{G}_t be an arbitrary network, and begin by assuming that the **entire network process** $\{\mathcal{G}_t : 0 < t < T_{\max}\}$ is fully observed. Explicitly accounting for the number of infectious contacts per individual at the time of infection as well as the total number of S - I links in the system, the complete data likelihood becomes:

$$\mathcal{L}(\beta, \gamma|\mathcal{G}) = \gamma^{n_R} \prod_{k=2}^{n_E} [\beta I_k(i_k)] \exp\left(-\int_0^{T_{\max}} [\beta SI(u) + \gamma I(u)] du\right). \quad (6)$$

Here $I_k(i_k)$ denotes the number of **infectious neighbors** of person k at his time of infection i_k and $SI(t)$ denotes the number of S - I links in the system at time t . We see that the dynamic nature of the network is implicitly subsumed into the terms $I_k(i_k)$'s and $SI(u)$. To clarify this point, note that the same likelihood holds for a *static* network \mathcal{G} . As neighborhoods $I_k(i_k)$ are fixed in the static case, one could further simplify (6) using a constant $I_k(i_k) = I_k$ for all times i_k .

Equation (6) serves as a point of departure toward network dynamics. As a stepping stone, we first consider the simpler **decoupled** case in which the network and epidemic evolve **independently**. Here the edge activation rate α and deletion rate ω , as well as total number of activated and terminated edges denoted C and D , do not depend on disease status. Given an initial network \mathcal{G}_0 , the network process likelihood can be easily written as

$$\begin{aligned} \mathcal{L}(\alpha, \omega|\mathcal{G}_0) &= p(\text{network events}|\alpha, \omega, \mathcal{G}_0) \\ &= \alpha^C \omega^D \prod_{\ell=1}^{n_N} \left[\left(\frac{N(N-1)}{2} - M(s_\ell) \right)^{1-D_\ell} M(s_\ell)^{D_\ell} \right] \end{aligned}$$

²Note that this expression differs from the **population-level** complete likelihood (Becker and Britton, 1999). When epidemic events are tied to individuals, i.e. a recovery time is associated to a specific infection event, we must use the individual-based likelihood instead (similar to that in Auranen et al. (2000)).

$$\times \exp\left(-\alpha \frac{N(N-1)}{2} T_{\max} + (\alpha - \omega) \int_0^{T_{\max}} M(u) du\right). \quad (7)$$

Here s_ℓ is the time of the ℓ th network event, and $D_\ell = 1$ if this event is a **link termination** and otherwise $D_\ell = 0$. By independence, the complete data likelihood in this decoupled case is simply a product of Equations (6) and (7):

$$\begin{aligned} \mathcal{L}(\beta, \gamma, \alpha, \omega | \mathcal{G}_0) &= p(\text{epidemic events} | \beta, \gamma, \mathcal{G}_t) \cdot p(\text{network events} | \alpha, \omega, \mathcal{G}_0) \\ &= \beta^{n_E-1} \gamma^{n_R} \alpha^C \omega^D \prod_{k=2}^{n_E} [I_k(i_k)] \prod_{\ell=1}^{n_N} \left[\left(\frac{N(N-1)}{2} - M(s_\ell) \right)^{1-D_\ell} M(s_\ell)^{D_\ell} \right] \\ &\quad \times \exp\left(-\int_0^{T_{\max}} [\beta SI(u) + \gamma I(u) + (\omega - \alpha)M(u)] du - \alpha \frac{N(N-1)}{2} T_{\max}\right). \end{aligned} \quad (8)$$

Finally, we allow link activation and termination to be dependent on individual disease status, yielding an **adaptive** network. We introduce some notation; it is natural to assume that the S and R populations behave identically from the perspective of the network process:

$$\alpha_{RA} \equiv \alpha_{SA}, \text{ and } \omega_{RA} \equiv \omega_{SA}, \forall A \in \{S, I, R\}.$$

Let $H(t) = R(t) + S(t) = N - I(t)$ denote the number of such “healthy” individuals at time t . Naturally the term “ H - H link” represent an S - S link, an S - R link, or an R - R link, and the term “ H - I link” represents an S - I link or R - I link. We also define $g(p, t)$ as the indicator function of infectiousness, i.e. $g(p, t) = 1$ if person p is infected at time t and $g(p, t) = 0$ otherwise.

Denote the ordered epidemic and network events together as $\{e_j = (t_j, p_{j1}, p_{j2})\}_{j=1}^n$, with $n = n_E + n_R + n_N$. Here t_j ($j = 1, 2, \dots, n$) denote the event times and $t_1 = 0$ is the infection time of the first patient. If e_j is a network event, p_{j1} and p_{j2} are the two individuals getting connected or disconnected, and if e_j is an epidemic event, let p_{j1} be the person getting infected or recovered and set $p_{j2} = 0$. Furthermore let event type indicators F_j, C_j, D_j take the value 1 only if e_j is an infection, a link activation, and a link deletion, respectively, and 0 otherwise.

The contribution of all network events to the complete data likelihood is in essence of the same form as (7), except that for every activation or termination event the link type has

to be considered. Then the likelihood component of the adaptive network process is

$$\alpha_{SS}^{C_{HH}} \alpha_{SI}^{C_{HI}} \alpha_{II}^{C_{II}} \omega_{SS}^{D_{HH}} \omega_{SI}^{D_{HI}} \omega_{II}^{D_{II}} \prod_{j=2}^n \tilde{M}(t_j) \exp \left(- \int_0^{T_{\max}} [\tilde{\alpha}^T \mathbf{M}_{\max}(t) + (\tilde{\omega} - \tilde{\alpha})^T \mathbf{M}(t)] dt \right),$$

where

$$\begin{aligned} \tilde{M}(t_j) &= [(\alpha_{SS} M_{HH}^d(t_j))^{C_j} (\omega_{SS} M_{HH}(t_j))^{D_j}]^{(1-g(p_{j1}, t_j))(1-g(p_{j2}, t_j))} \\ &\quad \times [(\alpha_{SI} M_{HI}^d(t_j))^{C_j} (\omega_{SI} M_{HI}(t_j))^{D_j}]^{|g(p_{j1}, t_j) - g(p_{j2}, t_j)|} \\ &\quad \times [(\alpha_{II} M_{II}^d(t_j))^{C_j} (\omega_{II} M_{II}(t_j))^{D_j}]^{g(p_{j1}, t_j)g(p_{j2}, t_j)} \end{aligned} \quad (9)$$

$$\tilde{\alpha} = (\alpha_{SS}, \alpha_{SI}, \alpha_{II})^T, \quad (10)$$

$$\tilde{\omega} = (\omega_{SS}, \omega_{SI}, \omega_{II})^T, \quad (11)$$

$$\mathbf{M}_{\max}(t) = \left(\frac{H(t)(H(t) - 1)}{2}, H(t)I(t), \frac{I(t)(I(t) - 1)}{2} \right)^T, \quad (12)$$

$$\mathbf{M}(t) = (M_{HH}(t_j), M_{HI}(t), M_{II}(t))^T. \quad (13)$$

Therefore, given the initial network structure \mathcal{G}_0 and one infectious case at time 0, the complete data likelihood of the coupled process can be expressed as ³

$$\begin{aligned} \mathcal{L}(\beta, \gamma, \tilde{\alpha}, \tilde{\omega} | \mathcal{G}_0) &= p(\text{epidemic events, network events} | \beta, \gamma, \tilde{\alpha}, \tilde{\omega}, \mathcal{G}_0) \\ &= \gamma^{n_R} \beta^{n_E - 1} \alpha_{SS}^{C_{HH}} \alpha_{SI}^{C_{HI}} \alpha_{II}^{C_{II}} \omega_{SS}^{D_{HH}} \omega_{SI}^{D_{HI}} \omega_{II}^{D_{II}} \prod_{j=2}^n \left[\tilde{M}(t_j) (I_{p_{j1}}(t_j))^{F_j} \right] \\ &\quad \times \exp \left(- \int_0^{T_{\max}} [\beta SI(t) + \gamma I(t) + \tilde{\alpha}^T \mathbf{M}_{\max}(t) + (\tilde{\omega} - \tilde{\alpha})^T \mathbf{M}(t)] dt \right). \end{aligned} \quad (14)$$

Inference Given Complete Event Data The likelihood function (14) will be used toward inference under missing data, but immediately suggests straightforward procedures when the process is fully observed. Given the complete event data $\{e_j\}_{j=1}^n$ and the initial conditions of the process \mathcal{G}_0 and $I(0)$, the only unknown quantities in (14) are the model parameters $\Theta = \{\beta, \gamma, \alpha_{SS}, \alpha_{SI}, \alpha_{II}, \omega_{SS}, \omega_{SI}, \omega_{II}\}$. The following Theorems state results on maximum likelihood estimation as well as Bayesian estimation.

³The likelihood derived here can be slightly modified to describe an SIS-type epidemic instead; see Supplement S1.

Theorem 3.1 (Maximum likelihood estimation). *Following the likelihood function in (14), given \mathcal{G}_0 and complete event data $\{e_j\}$, the MLEs of the model parameters are given as follows:*

$$\begin{aligned}\hat{\beta} &= \frac{n_E - 1}{\sum_{j=1}^n SI(t_j)(t_j - t_{j-1})}, & \hat{\gamma} &= \frac{n_R}{\sum_{j=1}^n I(t_j)(t_j - t_{j-1})}, \\ \hat{\alpha}_{SS} &= \frac{C_{HH}}{\sum_{j=1}^n \left[\frac{H(t_j)(H(t_j)-1)}{2} - M_{HH}(t_j) \right] (t_j - t_{j-1})}, & \hat{\omega}_{SS} &= \frac{D_{HH}}{\sum_{j=1}^n M_{HH}(t_j)(t_j - t_{j-1})}, \\ \hat{\alpha}_{SI} &= \frac{C_{HI}}{\sum_{j=1}^n [H(t_j)I(t_j) - M_{HI}(t_j)] (t_j - t_{j-1})}, & \hat{\omega}_{SI} &= \frac{D_{HI}}{\sum_{j=1}^n M_{HI}(t_j)(t_j - t_{j-1})}, \\ \hat{\alpha}_{II} &= \frac{C_{II}}{\sum_{j=1}^n \left[\frac{I(t_j)(I(t_j)-1)}{2} - M_{II}(t_j) \right] (t_j - t_{j-1})}, & \hat{\omega}_{II} &= \frac{D_{II}}{\sum_{j=1}^n M_{II}(t_j)(t_j - t_{j-1})}.\end{aligned}$$

The above results can be directly obtained by setting all partial derivatives of the log-likelihood to zero. The detailed proof is provided in Supplement S2.

Theorem 3.2 (Bayesian inference with conjugate priors). *Under Gamma priors*

$$\beta \sim Ga(a_\beta, b_\beta), \quad \gamma \sim Ga(a_\gamma, b_\gamma), \quad \alpha_{..} \sim Ga(a_\alpha, b_\alpha), \quad \omega_{..} \sim Ga(a_\omega, b_\omega)$$

and given initial network \mathcal{G}_0 and complete data $\{e_j\}$, the posterior distributions of model parameters under likelihood (14) are given by

$$\begin{aligned}\beta|\{e_j\} &\sim Ga(a_\beta + (n_E - 1), b_\beta + (n_E - 1)/\hat{\beta}), & \gamma|\{e_j\} &\sim Ga(a_\gamma + n_R, b_\gamma + n_R/\hat{\gamma}), \\ \alpha_{SS}|\{e_j\} &\sim Ga(a_\alpha + C_{HH}, b_\alpha + C_{HH}/\hat{\alpha}_{SS}), & \omega_{SS}|\{e_j\} &\sim Ga(a_\omega + D_{HH}, b_\omega + D_{HH}/\hat{\omega}_{SS}), \\ \alpha_{SI}|\{e_j\} &\sim Ga(a_\alpha + C_{HI}, b_\alpha + C_{HI}/\hat{\alpha}_{SI}), & \omega_{SI}|\{e_j\} &\sim Ga(a_\omega + D_{HI}, b_\omega + D_{HI}/\hat{\omega}_{SI}), \\ \alpha_{II}|\{e_j\} &\sim Ga(a_\alpha + C_{II}, b_\alpha + C_{II}/\hat{\alpha}_{II}), & \omega_{II}|\{e_j\} &\sim Ga(a_\omega + D_{II}, b_\omega + D_{II}/\hat{\omega}_{II}),\end{aligned}\tag{15}$$

where $\hat{\beta}, \hat{\gamma}, \hat{\alpha}_{SS}, \hat{\alpha}_{SI}, \hat{\alpha}_{II}, \hat{\omega}_{SS}, \hat{\omega}_{SI}, \hat{\omega}_{II}$ are the MLEs defined in Theorem 3.1.

Equation (14) is consistent with the general form of likelihood of a continuous-time Markov chain with Exponentially distributed dwell times. Applying the Gamma-Exponential conjugacy leads to the posterior distributions in (15).

Relaxing the closed population assumption Above, the host population was implicitly assumed to be closed by fixing N . If in reality the observed population of size N is a subset

of a larger unobserved population, then it is possible for an individual to get infected by an external source. This is not reflected in the likelihood above as there is no corresponding S - I link within the observed population, so we introduce an “external infection” rate ξ describing the rate for each susceptible individual to contract the disease from an external source. In other words, ξ can be thought of as the constant rate for any S individual to enter status I independently of interaction with infectious members in the observed population. In this scenario, the complete data likelihood becomes

$$\begin{aligned} \mathcal{L}(\beta, \xi, \gamma, \tilde{\alpha}, \tilde{\omega} | \mathcal{G}_0) &= \gamma^{n_R} \alpha_{SS}^{C_{HH}} \alpha_{SI}^{C_{HI}} \alpha_{II}^{C_{II}} \omega_{SS}^{D_{HH}} \omega_{SI}^{D_{HI}} \omega_{II}^{D_{II}} \prod_{j=2}^n \left[\tilde{M}(t_j) (\beta I_{p_{j1}}(t_j) + \xi)^{F_j} \right] \\ &\times \exp \left(- \int_0^{T_{\max}} [\beta SI(t) + \xi S(t) + \gamma I(t) + \tilde{\alpha}^T \mathbf{M}_{\max}(t) + (\tilde{\omega} - \tilde{\alpha})^T \mathbf{M}(t)] dt \right). \end{aligned}$$

The MLEs for $\{\gamma, \tilde{\alpha}, \tilde{\omega}\}$ remain unchanged, and though there is no longer a closed-form solution to the MLEs for β and ξ , numerical solutions can be easily obtained as detailed in Supplement S3. In particular, if we have information on which infection cases are caused by internal sources (described by β) and which are caused by external sources (described by ξ), we can directly obtain the MLEs (and posterior distributions) for all the parameters. In this case, estimation for all parameters except β and ξ remains unchanged. When there is missingness in recovery times, the Bayesian inference procedure proposed in the next section can still be carried out with only minor adaptations.

4 Inference with Partial Epidemic Observations

Though likelihood-based inference is straightforward when all events are observed, complete event data are rarely collected in real-world epidemiological studies. Even in epidemiological studies with very comprehensive observations (Aiello et al., 2016), there still exists some degree of missingness in the exact individual recovery times. In these data, infection times are recorded when a study subject reports symptoms, but recoveries are aggregated at a coarse time scale rather than immediately recorded when a subject becomes disease-free.

Incomplete observations on epidemic paths have long been a major challenge for inference, even assuming a randomly mixing population or a simple, fixed network structure. With the

exact times of infections and/or recoveries unknown, it essentially requires integrating over all possible individual disease episodes to obtain the **marginal** likelihood of the parameters. In most cases, this is intractable. Instead, our strategy is to bypass the direct marginalization through data augmentation. This entails treating the unknown quantities in data as latent variables, iteratively imputing their values, and then estimating parameters given the current setting of latent variables. By **augmenting** the data via latent variables, the parameter estimation step makes use of the computationally tractable complete-data likelihood. This class of methods has proven successful for related problems based on individual-level data (Auranen et al., 2000; Höhle and Jørgensen, 2002; Cauchemez et al., 2006; Hoti et al., 2009; Tsang et al., 2019), population-wide prevalence counts (Fintzi et al., 2017), and observations on a structured but static population (Neal and Roberts, 2004; O’Neill, 2009; Tsang et al., 2019), but has not yet been designed for an epidemic process coupled with a **dynamic** network. The time-varying nature of social interactions imposes complex constraints on the data augmentation. Though network dynamics complicate the design of data-augmented samplers, the information they provide on possible infection sources and transmission routes allow us to exploit additional structure, effectively reducing the size of the latent space.

We derive a data augmentation method specifically designed to enable inference under missing recovery times. The algorithm utilizes the information presented by the dynamic contact structure. In contrast to existing methods (such as Fintzi et al. (2017) and Hoti et al. (2009)), it is able to efficiently impute unobserved event times in parallel instead of updating individual trajectories one by one. We focus on the case when recovery times are missing, directly motivated by the case study data in Section 6, but note that the proposed framework applies to other sources of missing data; see Section 7 for discussion.

4.1 Method Overview

Problem setting Throughout the observation period $(0, T_{\max}]$, suppose $\{(u_\ell, v_\ell]\}_{\ell=1}^L$ ($u_\ell < v_\ell$ and $v_\ell \leq u_{\ell+1}$) is the collection of **disjoint** time intervals in which a certain number of recoveries occur, but the exact times of those recoveries are unknown. That is, for each $\ell = 1, 2, \dots, L$, some individuals are reported as infectious up to time u_ℓ , and they are reported as healthy again starting from time v_ℓ . Within one particular interval $(u_\ell, v_\ell]$, let

$n_E^{(\ell)}$ be the number of infections, and $n_R^{(\ell)}$ the number of recoveries for which the **exact times are known**, so the number of **unknown** recovery times for this interval is $R_\ell = I(u_\ell) - I(v_\ell) + n_E^{(\ell)} - n_R^{(\ell)}$. Denote these recovery times by latent variables $\mathbf{r}_\ell = \{r_{\ell,1}, \dots, r_{\ell,R_\ell}\}$. Our goal is to conduct inference despite the absence of all the exact recovery times $\mathbf{r} = \{\mathbf{r}_\ell\}_{\ell=1:L}$ in the observed data.

Further assume that we have a health status report (indicating ill or healthy) of each individual periodically during $(0, T_{\max}]$. Access to such information is usually granted in epidemiological studies where every study subject gives updates on health statuses through regular surveys (for example, weekly surveys).

Inference scheme We propose to address the problem of missing recovery times through data-augmented Markov chain Monte Carlo. Given an initial guess of parameter values $\Theta^{(0)}$ and the observed data $\mathbf{x} = \{e_j\} \cup \{\text{health status reports}\} \cup \mathcal{Z}_0$, at each iteration s the algorithm samples a set of values for the missing recovery times $\mathbf{r}^{(s)} = \{\mathbf{r}_\ell^{(s)}\}_{\ell=1:L}$ from their probability distribution conditioned on \mathbf{x} and the current draw of parameter values. It then samples a new set of parameter values $\Theta^{(s)}$ from their posterior distributions conditioned on the augmented data. In summary, for $s = 1 : S$ where S is the maximum iteration count:

1. **Data augmentation.** Draw $\mathbf{r}^{(s)} = \{\mathbf{r}_\ell^{(s)}\}_{\ell=1:L}$ from the joint conditional distribution

$$p(\mathbf{r} | \Theta^{(s-1)}, \mathbf{x}, \mathbf{r}^{(s-1)}). \quad (16)$$

2. **Parameter update.** Combine \mathbf{x} and $\mathbf{r}^{(s)}$ to form the augmented, complete data. Sample parameters $\Theta^{(s)} | \mathbf{x}, \mathbf{r}^{(s)}$ according to (15).

4.2 Data Augmentation via Endpoint-conditioned Sampling

In the inference scheme stated above, the data augmentation step (step 1) is challenging because (16) describes the distribution of missing recovery times conditioned on both historical events **and** future events. Thus drawing from (16) amounts to sampling unobserved event times from a continuous-time Markov process with a series of fixed endpoints (Hobolth and Stone, 2009), a challenging task. Even though (3) suggests that, in **forward simulations**, the time it takes for an infectious person to recover only depends on the recovery rate

γ , when recovery times need to be inferred **retrospectively**, there are additional constraints imposed by the observed data. First, an individual q cannot recover before a certain time point t if it is observed that at time t the person is still ill. More subtly, if another individual p gets infected during his contact with q , then the associated recovery time for q cannot leave p without a possible infection source. The first condition is easy to satisfy. The second constraint is much more complicated due to the network dynamics, which a simple forward simulation approach would fail to effectively accommodate.

We tackle the challenge in data augmentation by first simplifying the expression of (16) and then stating an efficient sampling algorithm.

Lemma 4.1. (16) can be simplified into the following expression:

$$\prod_{\ell=1:L} p(\mathbf{r}_\ell | \gamma^{(s-1)}, \{e_j\}_{t_j \in (u_\ell, v_\ell]}, \mathcal{Z}_{u_\ell}), \quad (17)$$

where \mathcal{Z}_t is the state of the process at time t , including the epidemic status of each individual and the social network structure.

Proof. Consider the joint density of the complete data given parameter values $\Theta^{(s-1)}$.

$$\begin{aligned} & p(\mathbf{x}, \{\mathbf{r}_\ell\}_{\ell=1:L} | \Theta^{(s-1)}) \\ &= \prod_{\ell=1:L} [p(\{e_j\}_{t_j \in (u_\ell, u_{\ell+1}]}, \mathbf{r}_\ell | \mathcal{Z}_{u_\ell}, \Theta^{(s-1)})] \times p(\{e_j\}_{t_j \leq u_1 \text{ or } t_j > v_L} | \mathcal{Z}_0, \mathcal{Z}_{v_L}, \Theta^{(s-1)}) \\ &= \prod_{\ell=1:L} [p(\{e_j\}_{t_j \in (u_\ell, v_\ell]} | \mathbf{r}_\ell, \mathcal{Z}_{u_\ell}, \Theta^{(s-1)}) p(\mathbf{r}_\ell | \mathcal{Z}_{u_\ell}, \gamma^{(s-1)})] \\ & \quad \times \left[\prod_{\ell=1:L} p(\{e_j\}_{t_j \in (v_\ell, u_{\ell+1}]}, \mathcal{Z}_{v_\ell}, \Theta^{(s-1)}) \right] p(\{e_j\}_{t_j \leq u_1 \text{ or } t_j > v_L} | \mathcal{Z}_0, \mathcal{Z}_{v_L}, \Theta^{(s-1)}). \end{aligned}$$

Examining all terms concerning \mathbf{r}_ℓ for each ℓ indicates that, conditioned on $\gamma^{(s-1)}$, $\{e_j\}_{t_j \in (u_\ell, v_\ell]}$, and \mathcal{Z}_{u_ℓ} , the distribution of \mathbf{r}_ℓ does **not** depend on $\{\mathbf{r}_{\ell'}\}_{\ell' \neq \ell}$. Thus,

$$p(\mathbf{r} | \Theta^{(s-1)}, \mathbf{x}, \mathbf{r}^{(s-1)}) = \prod_{\ell=1:L} p(\mathbf{r}_\ell | \gamma^{(s-1)}, \{e_j\}_{t_j \in (u_\ell, v_\ell]}, \mathcal{Z}_{u_\ell}).$$

□

The lemma above suggests that imputation of missing recovery times inside an interval $(u, v]$ only depends on the events that occur in $(u, v]$, the state of the process at the start of

the interval, \mathcal{Z}_u , and the value of recovery rate γ . Further, imputation on disjoint intervals can be conducted separately and in parallel.

Now consider sampling recovery times within any interval $(u, v]$. Let \mathcal{Q} denote the group of individuals who recover at unknown times during $(u, v]$, and for each $q \in \mathcal{Q}$, let q 's exact recovery time be $r_q \in (u, v]$. Similarly, let \mathcal{P} denote the group of individuals who get infected during $(u, v]$; for $p \in \mathcal{P}$, let p 's infection time be i_p , $\mathcal{N}_p(i_p)$ be the set of p 's contacts at time i_p , and $\mathcal{I}(i_p)$ be the set of **known** infectious individuals at time i_p (that is, $\mathcal{I}(i_p)$ excludes any individual who may have recovered before i_p).

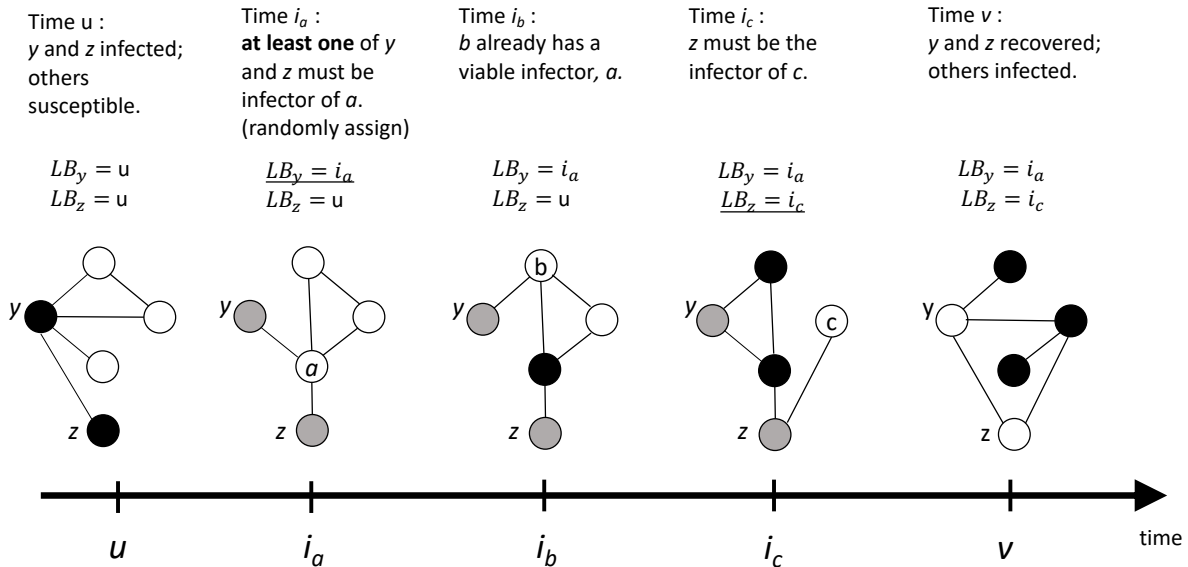


Figure 1: Illustration of DARCI on a $N = 5$ population. Each circle represents an individual and each solid line represents a link. Disease status is color-coded: dark = infectious, grey = unknown (possibly infectious or recovered), and white = healthy (susceptible or recovered). Individuals y and z are known to be infectious at time u but are recovered by time v , and individuals a , b and c are known to get infected at time points i_a , i_b and i_c , respectively. For each person $p \in \{a, b, c\}$, the DARCI algorithm inspects p 's contacts at infection time i_p , and updates “lower bounds” (LB) of y and z 's recovery times to ensure that p has an infector. For example, at time i_a , one of y and z has to be a 's infector, so DARCI randomly selects **one** of y and z (in this example it's y) and postpones his recovery time until after i_a .

Proposition 4.2 (Data augmentation regulated by contact information (DARCI)). *Following the notation stated above, given a recovery rate γ , the state of the process at time u , \mathcal{Z}_u , and all the observed events in the interval $(u, v]$, $\{e_j\}_{t_j \in (u, v]}$, one can sample $\{r_q\}$ from the conditional distribution $p(\{r_q\} | \gamma, \{e_j\}_{t_j \in (u, v]}, \mathcal{Z}_u)$ in the following steps:*

1. *Initialize a vector LB of length $|\mathcal{Q}|$ with $LB_q = u$ for every $q \in \mathcal{Q}$; then for any $p \in \mathcal{P}$ such that $p \in \mathcal{Q}$, further set $LB_p = u$;*
2. *Arrange the set \mathcal{P} in the order of $\{p_1, p_2, \dots, p_{|\mathcal{P}|}\}$ such that $i_{p_1} < i_{p_2} < \dots < i_{p_{|\mathcal{P}|}}$, and for each $p \in \mathcal{P}$ (chosen in the arranged order), examine the “potential infectious neighborhood”*

$$\mathcal{I}_p = \mathcal{N}_p(i_p) \cap (\mathcal{I}(i_p) \cup \mathcal{Q}).$$

If $\mathcal{I}_p \subset \mathcal{Q}$ (i.e., potential infection sources are all members of \mathcal{Q}), then randomly and uniformly select one $q \in \mathcal{I}_p$, and set $LB_q = i_p$.

3. *Draw recovery times $r_q \stackrel{\text{ind}}{\sim} \text{TEXP}(\gamma, LB_q, v)$, where $\text{TEXP}(\gamma, s, t)$ is a truncated Exponential distribution with rate γ and truncated on the interval (s, t) .*

Intuitively, this procedure enables a draw of recovery times that are “consistent with” the observed data. To achieve this goal, an imputed recovery cannot occur in a way that leaves a to-be-infected individual without any infectious neighbor at the time of infection, nor take place before the corresponding individual gets infected. Effectively there is a “lower bound” for each missing recovery time conditioned on the observed data, particularly the dynamic contact structure. An illustration of the DARCI algorithm is provided in Figure 1.

Combining Lemma 4.1 and Proposition 4.2 enables exact sampling from the conditional distribution (17) in the data augmentation step: for each $\ell = 1, 2, \dots, L$, applying the DARCI algorithm to the interval $(u_\ell, v_\ell]$ gives an updated set of missing recovery times, $\mathbf{r}^\ell = \{r_{\ell, i}\}_{i=1:R_\ell}$. This allows us to carry out MCMC sampling using a simple Gibbs sampler.

5 Simulation Experiments

In this section we present results of a series of experiments with simulated datasets. In all experiments, we employ a forward simulation procedure that can be seen as a variation of Gillespie’s algorithm (Gillespie, 1976) to sample realizations of the network epidemic from our generative model. The input consists of the parameter values $\Theta = \{\beta, \gamma, \tilde{\alpha}, \tilde{\omega}\}$ ⁴, an arbitrary initial network \mathcal{G}_0 , the number of infectious cases at onset $I(0)$, and the observation time length T_{\max} . The output is the complete collection of all events $\{e_j = (t_j, p_{j1}, p_{j2}, F_j, C_j, D_j)\}$ that occur within the time interval $(0, T_{\max}]$. Associated with each event e_j is a timestamp (t_j), labels of the individuals involved (p_{j1}, p_{j2}), and the event-type indicator F_j, C_j , or D_j .

The steps of the simulation procedure are detailed as follows:

1. **Initialization.** Randomly select $I(0)$ individuals to be the infectious (then the rest of the population are all susceptible). Set $t_{\text{cur}} = 0$.
2. **Iterative update.** While $t_{\text{cur}} < T_{\max}$, do:
 - (a) **Bookkeeping.** Summarize the following statistics at t_{cur} : 1) $SI(t_{\text{cur}})$, the number of S-I links in the population; 2) $\mathbf{M}_{\max}(t_{\text{cur}})$, the possible number of links of each type defined in (12); 3) $\mathbf{M}(t_{\text{cur}})$, the number of existing links of each type defined in (13). Then set $\mathbf{M}^d(t_{\text{cur}}) = \mathbf{M}_{\max}(t_{\text{cur}}) - \mathbf{M}(t_{\text{cur}})$.
 - (b) **Next event time.** Compute the instantaneous rate of the occurrence of any event, $\Lambda(t_{\text{cur}}) = \beta SI(t_{\text{cur}}) + \gamma I(t_{\text{cur}}) + \tilde{\alpha}^T \mathbf{M}^d(t_{\text{cur}}) + \tilde{\omega}^T \mathbf{M}(t_{\text{cur}})$, and draw $\Delta t \sim \text{Exponential}(\Lambda(t_{\text{cur}}))$.
 - (c) **Next event type.** Sample $Z \sim \text{Multinomial}(\tilde{\lambda}(t_{\text{cur}}))$, where

$$\tilde{\lambda}(t_{\text{cur}}) = \left(\frac{\beta SI(t_{\text{cur}})}{\Lambda(t_{\text{cur}})}, \frac{\gamma I(t_{\text{cur}})}{\Lambda(t_{\text{cur}})}, \frac{\tilde{\alpha}^T \mathbf{M}^d(t_{\text{cur}})}{\Lambda(t_{\text{cur}})}, \frac{\tilde{\omega}^T \mathbf{M}(t_{\text{cur}})}{\Lambda(t_{\text{cur}})} \right)^T.$$

Then do one of the following based on the value of Z :

If $Z = 1$ (infection), uniformly pick one S - I link and infect the S individual in this link.

If $Z = 2$ (recovery), uniformly pick one I individual to recover.

⁴Here $\tilde{\alpha} = (\alpha_{SS}, \alpha_{SI}, \alpha_{II})^T$ and $\tilde{\omega} = (\omega_{SS}, \omega_{SI}, \omega_{II})^T$, as defined in (10) and (11).

If $Z = 3$ (link activation), randomly select $Y \in \{H-H, H-I, I-I\}$ with probabilities proportional to $\tilde{\alpha} \circ \mathbf{M}^d(t_{\text{cur}})$, and uniformly pick one de-activated “ Y link” to activate.

If $Z = 4$ (link termination), randomly select $Y \in \{H-H, H-I, I-I\}$ with probabilities proportional to $\tilde{\omega} \circ \mathbf{M}(t_{\text{cur}})$, and uniformly pick one existing “ Y link” to terminate.

- (d) Replace t_{cur} by $t_{\text{cur}} + \Delta t$, record relevant information about the sampled event, and repeat from (a).

In Step 2 (c), “ \circ ” refers to the Hadamard product (entrywise product) for two vectors.

5.1 Experiments with Complete Observations

In this subsection, we first demonstrate the insufficiency of analyzing disease spread without considering the network structure or its dynamics. Then we validate our claims on maximum likelihood estimation and Bayesian inference given complete event data (Theorems 3.1 and 3.2). Finally, we show that the model estimators can detect simpler models such as the decoupled process and the static network process. Unless otherwise stated, throughout this section we set the initial network \mathcal{G}_0 as a random Erdős–Rényi graph⁵ (undirected) with edge probability $p = 0.1$, let $I(0) = 1$ individual to get infected at onset, and choose the ground-truth parameters as

$$\beta = 0.03, \gamma = 0.12; \tilde{\alpha}^T = (0.005, 0.001, 0.005), \tilde{\omega}^T = (0.05, 0.1, 0.05). \quad (18)$$

These settings are chosen to produce simulated data sets with a population size and event counts that are comparable to our real data example.

For Bayesian inference, we adopt the following Gamma priors for the parameters:

$$\beta \sim Ga(1, 1/0.02), \gamma \sim Ga(1, 1/0.1); \alpha_{..} \sim Ga(1, 1/0.004), \omega_{..} \sim Ga(1, 1/0.06). \quad (19)$$

⁵We note that the form of the initial network does not necessarily predict the behavior of the epidemic. Specifically, asymptotic qualities, such as the Poisson degree distribution of Erdős–Rényi graphs, do not hold when the network dynamically reacts to an epidemic, detailed empirically in Section Supplement S4.

We intentionally choose prior means different from the true parameter values; experiments show that inference is insensitive to prior specifications as long as a reasonable amount of data is available. For each parameter, 1000 posterior samples are drawn after a 200-iteration burn-in period.

The danger of neglecting networks or network dynamics Adopting the “random mixing” assumption about an actually networked population can lead to severe underestimation of the infection rate. Erroneous estimation can also happen if contacts are in fact dynamic but are mistaken as static during inference. Table 2 displays the MLEs of the infection rate β (**under true value 0.05**, chosen to generate non-trivial epidemics to illustrate inference) obtained by methods under three different assumptions regarding the network structure (assuming a dynamic network, assuming a static network, and assuming random mixing without any network). The population size is $N = 50$, and results are summarized over 50 different simulated datasets.

These results make clear that neglecting the effects of the contact network, even when the quantity of interest is the disease transmission rate, is dangerously misleading. Resulting estimates that are far from the truth with significantly underestimated uncertainty measures. Incorporating the initial network structure statically throughout the process helps—the 95% confidence interval now includes the truth—but disregarding the time-evolution of the network remains a noticeable model misspecification leading to biased inference.

Table 2: Maximum likelihood estimates of β , the per link infection rate (real value 0.05), using dynamic network information, the initial static network, and no network structure (random mixing), respectively. The standard deviations as well as the 2.5% and 97.5% quantiles of the estimates are obtained from outcomes across 50 different simulated datasets on a $N = 50$ population.

Method	dynamic network	static network	no network
Estimate	0.0540	0.0278	0.00219
Standard deviation	0.0158	0.0081	0.000821
2.5% quantile	0.0230	0.00825	0.000614
97.5% quantile	0.0817	0.0553	0.00425

Validity and efficacy of parameter estimation Complete event data are generated using the simulation procedure stated in above, and maximum likelihood estimates (MLEs) as well as Bayesian estimates are obtained for parameters $\Theta = \{\beta, \gamma, \tilde{\alpha}, \tilde{\omega}\}$. Here we set the population size as $N = 100$ and the infection rate as $\beta = 0.03$ while keeping the other parameter values the same as stated in (18).

Figure 2 shows the results of maximum likelihood estimation in one simulated dataset. The MLEs for the each parameter (dark solid line) are computed using various numbers of events, and are compared with the true parameter value (red horizontal lines). The lower and upper bounds for 95% confidence intervals are also calculated (dashed gray lines). Only the MLEs for parameters $\beta, \gamma, \alpha_{SS}$ and α_{SI} are shown, but results for all parameters are included in Supplement S5. Estimation is relatively accurate even when observation ends earlier than the actual process (thus leaving later events unobserved). When more events are available for inference, accuracy is improved and the uncertainty is reduced.

Figure 3 presents the posterior sample means (solid lines) and 95% credible bands (shades) for each parameter inferred using various numbers of events, with the true parameter values marked by bold, dark horizontal lines. The results are shown for 4 different simulated datasets (each dataset represented by a distinct color) and for parameters $\beta, \gamma, \omega_{SS}$ and ω_{SI} (complete results are in Supplement S5). When more events are utilized in inference, the posterior means tend to be closer to the true parameter values, while the credible bands gradually narrow down.

It is worth noting that the proposed inferential framework is capable of handling large-scale networks as well as arbitrary network structures. Additional results with larger values of N and different configurations of \mathcal{G}_0 are provided in Supplement S5.

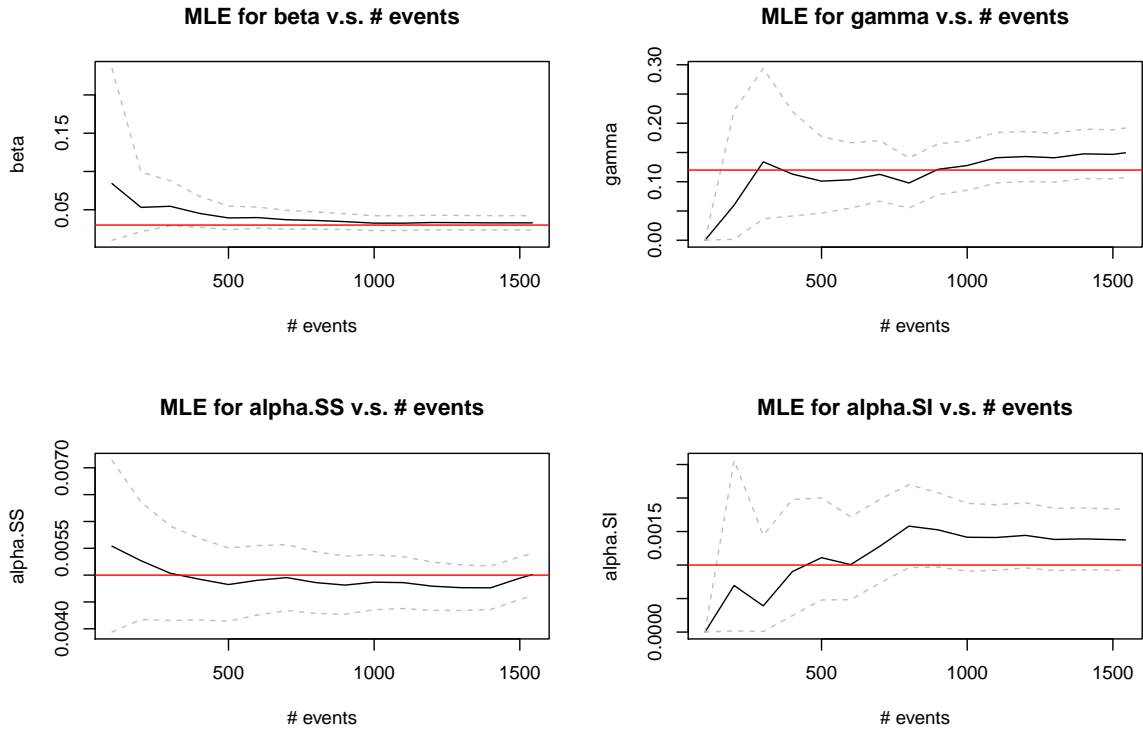


Figure 2: MLEs versus number of events used for inference. Dashed gray lines show the lower and upper bounds for 95% frequentist confidence intervals, and red lines mark the true parameter values. Results are presented for $\beta, \gamma, \alpha_{SS}$ and α_{SI} . In this realization $n_E = n_R = 48, C_{HH} = 621, C_{HI} = 35, C_{II} = 13, D_{HH} = 573, D_{HI} = 189, D_{II} = 17$.

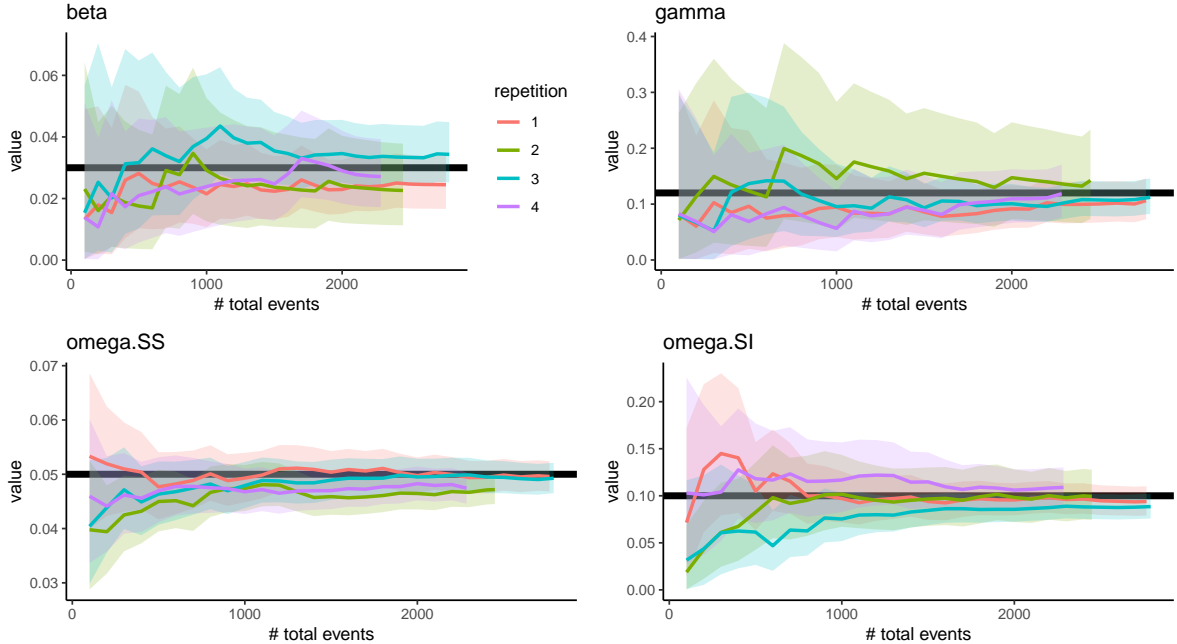


Figure 3: Posterior sample means versus number of total events used for inference. True parameter values are marked by **bold dark** horizontal lines, along with 95% credible bands. Results are presented for 4 different complete datasets and for parameters $\beta, \gamma, \omega_{SS}$ and ω_{SI} .

Assessing model flexibility Our proposed framework is a generalization of epidemics over networks that evolve independently (the “decoupled” process), which in turn generalize epidemic processes over fixed networks (the “static network” process). Thus our model class contains these simpler models: if events are generated from the decoupled process, we would expect all the link activation and termination rates to be estimated as the same. Likewise, if the true network process is static, then we expect all link rates to be estimated as zero.

To confirm this, experiments are conducted on complete event datasets generated from the two simpler models. Here we only show select results of Bayesian inference on datasets generated from static network epidemic processes (Figure 4) and relegate other results to Supplement S5. We see that information from a moderate number of events is sufficient to accurately estimate the epidemic parameters β and γ and learn the static nature of the network—note how quickly the posterior credible bands for α_{SI} and ω_{SI} shrink toward zero.

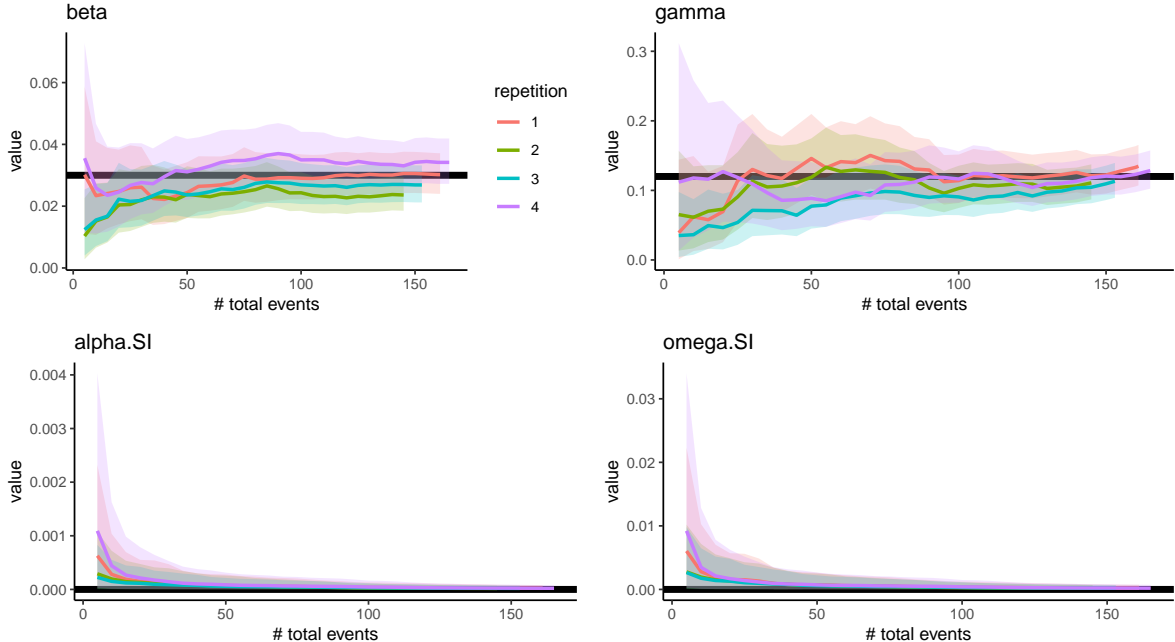


Figure 4: Posterior sample means versus number of total events used for inference, with data generated from *static* network epidemic processes. True parameter values are marked by **bold dark** horizontal lines, along with 95% credible bands. Results are presented for 4 different complete datasets and for parameters $\beta, \gamma, \alpha_{SI}$ and ω_{SI} . With a moderate number of events, the epidemic-related parameters, β and γ , are accurately estimated, and the posteriors for the edge rates quickly shrink toward zero (the truth).

5.2 Experiments with Incomplete Observations

Upon validating the model and inference framework, we now assess the performance of our proposed inference scheme in the more realistic setting where epidemic observations are incomplete. In this subsection, we first verify that the MCMC sampling scheme in Section 4 is able to retrieve the parameter values despite missing recovery times in the observed data. Then we compare our DARCI algorithm (Prop. 4.2) with two baselines and show that it produces posterior samples of higher quality and with higher efficiency.

Simulating partially observed data We first generate complete event data using the simulation procedure stated earlier in this section, and then randomly discard $\eta \times 100\%$ of the **exact** recovery times and treat them as unknown. Meanwhile, a periodic status report

(as described in Section 4.1) is produced every 7 time units throughout the entire process so that individual disease statuses are informed at a coarse resolution. If one regards 1 time unit as *a day*, the periodical disease statuses correspond to *weekly* reports.

Efficacy of the inference scheme We validate the method outlined in Section 4.1 through experiments on an example dataset, where the settings and parameters are the same as those in (18) and the population size is fixed at $N = 100$. In this particular realization, there are 26 infection cases spanning over approximately 37 days (less than 6 weeks), and there are 767 and 893 instances of social link activation and termination, respectively.⁶

First set $\eta = 50$, that is, randomly select 50% of exact recovery times to be taken as missing. Figure 5 plots 1000 consecutive MCMC samples (after a 200-iteration burn-in) for each parameter $\{\beta, \gamma, \alpha_{SS}, \omega_{SS}\}$, as well as the 2.5% and 97.5% quantiles of the posterior samples (gray, dashed lines) compared with the true parameter value (red horizontal line). We can see that for every parameter, the 95% sample credible interval covers the true parameter value, suggesting that the proposed inference scheme is able to estimate parameters from incomplete data reasonably well.

We then set $\eta = 100$, discarding all exact recovery times. Figure 6 presents outcomes of the inference algorithm in this case. Understandably, parameter estimation is affected by the total unavailability of exact recovery times, but the drop in accuracy is marginal. Moreover, the credible bands are slightly wider, reflecting increased uncertainty with more missingness.

⁶The event time scales in the example dataset are chosen to be comparable to, though not exactly the same as, those in the real-world data used in Section 6.

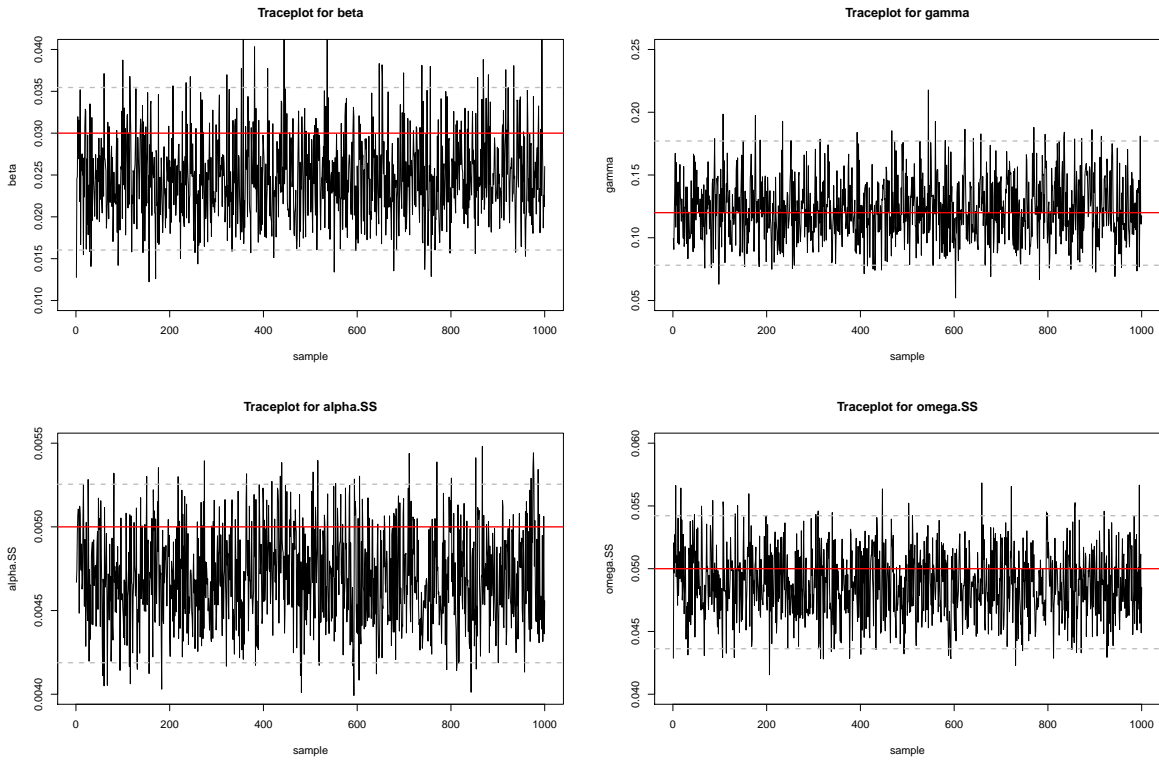


Figure 5: Inference results for parameters $\beta, \gamma, \alpha_{SS}, \omega_{SS}$ with 50% recovery time missingness. The uncertainty in exact recovery times does affect the estimation of the type-dependent edge rates, but not detrimentally (all the true parameter values fall into the 95% credible intervals of the posteriors).

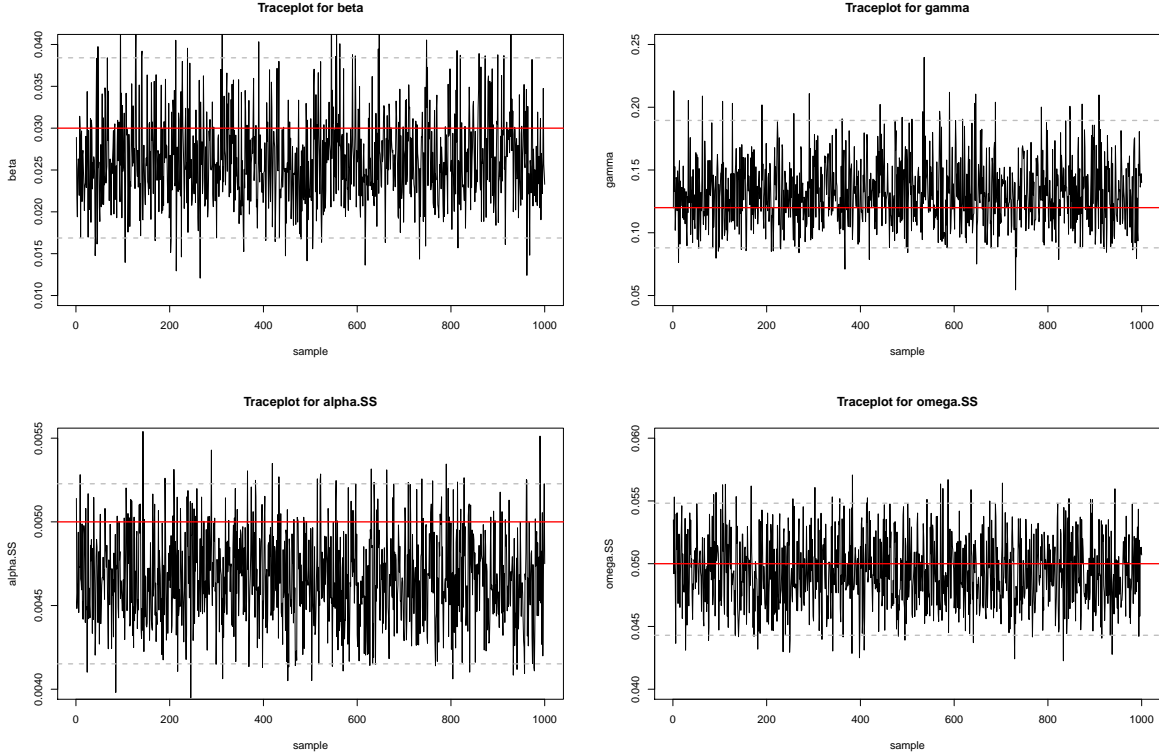


Figure 6: Inference results for parameters $\beta, \gamma, \alpha_{SS}, \omega_{SS}$ with complete (100%) missingness in exact recovery times. The y-axis scale for each plot is the same as that in Figure 5 for easier comparison. Wider credible intervals are seen for β and γ , but still, all the true parameter values fall into the 95% credible intervals of the posteriors, suggesting the capability of the inference algorithm to estimate parameters even when there is uncertainty in individual epidemic histories.

Efficiency of the DARCI algorithm We compare performance of the data augmentation algorithm stated in Proposition 4.2 with two conventional sampling methods:

1. **Rejection sampling:** Carry out Step 1 of the inference scheme via rejection sampling. For $\ell = 1 : L$, keep proposing recovery times $\mathbf{r}_\ell^* = \{r_{\ell,i}^*\}_{i=1:R_\ell} \stackrel{iid}{\sim} \text{TEXP}(\gamma^{(s-1)}, u_\ell, v_\ell)$ until the proposed \mathbf{r}_ℓ^* are compatible with the observed event data in $(u_\ell, v_\ell]$. We label this method by “**Reject**”.
2. **Metropolis-Hastings:** Modify Step 1 of the inference scheme into a Metropolis-Hastings step. For $\ell = 1 : L$, propose $\mathbf{r}_\ell^* = \{r_{\ell,i}^*\}_{i=1:R_\ell} \stackrel{iid}{\sim} \text{TEXP}(\gamma^{(s-1)}, u_\ell, v_\ell)$, and

accept them as $\mathbf{r}_\ell^{(s)}$ with probability

$$\min \left(1, \frac{p \left(\mathbf{x}, \mathbf{r}_\ell^*, \{\mathbf{r}_{\ell'}^{(s-1)}\}_{\ell' \neq \ell} | \Theta^{(s-1)} \right) \text{pTEXP} \left(\mathbf{r}_\ell^{(s-1)}; \gamma^{(s-1)}, u_\ell, v_\ell \right)}{p \left(\mathbf{x}, \{\mathbf{r}_{\ell'}^{(s-1)}\}_{\ell'=1:L} | \Theta^{(s-1)} \right) \text{pTEXP} \left(\mathbf{r}_\ell^*; \gamma^{(s-1)}, u_\ell, v_\ell \right)} \right),$$

which equals to 1 when the proposed \mathbf{r}_ℓ^* are consistent with the observed event data in $(u_\ell, v_\ell]$ and 0 otherwise. If the proposal is not accepted, then set $\mathbf{r}_\ell^{(s)} = \mathbf{r}_\ell^{(s-1)}$. We label this method by “**MH**”.

The “**MH**” method employs the same principle as existing agent-based data augmentation methods (Cauchemez et al., 2006; Hoti et al., 2009; Fintzi et al., 2017) that propose candidates of individual disease histories and accept them with probabilities computed through evaluating the likelihood (or an approximation of it) and the proposal density. In our case the implementation of “**MH**” is actually simpler and computationally lighter because the proposal is conditioned on known infection times and the current posterior draw of γ . The acceptance step is reduced to inspecting compatibility with known data, thus avoiding the intensive computation of likelihood evaluation.

Although the three methods give the same inference results since they all sample from the same posterior distributions, our data augmentation algorithm (labeled by “**DARCI**”) is more efficient than the others in two aspects. First, by drawing a new sample of recovery times from the conditional distribution in (16) in each iteration, the resulting Markov chain exhibits lower autocorrelation, which leads to better mixing and fewer iterations needed to achieve a certain effective sample size. This is especially so when compared with “**MH**”. Second, the DARCI algorithm typically draws from the conditional distribution (16) much more efficiently than “**Reject**”, because it parses out a configuration of lower bounds for imputing missing recovery times while accounting for the constraints imposed by contagion spreading and the dynamics of social links.

Three MCMC samplers are run using the three methods on the dataset showcased above. Again 1000 consecutive samples are retained for each parameter after a 200-iteration burn-in period in each case. For each parameter, we calculate the effective sample size (ESS), the Geweke Z-score (Geweke et al., 1991), and the two-sided p-value for the Z-scores of the resulting chains. These results are presented in Table 3. Among the three methods, “**MH**”

suffers the most from the correlation between two successive samples, while “**DARCI**” seems to produce high-quality MCMC samples.

Table 3: MCMC diagnostics for three data augmentation sampling methods, labelled as “**DARCI**”, “**Reject**”, and “**MH**”. “ESS” stands for “effective sample size”. The “Z-score” is the test statistic for MCMC convergence proposed by Geweke et al. (1991), and the two-sided p-value for each standard Z-score is also computed. Samples acquired by **MH** tend to have higher auto-correlations and thus smaller effective sample sizes.

Statistic	β	γ	α_{SS}	α_{SI}	α_{II}	ω_{SS}	ω_{SI}	ω_{II}	Method
ESS	1000.00	1000.00	1000.00	1000.00	1000.00	1000.00	1000.00	1000.00	
Z-score	-0.90	-0.20	-0.56	-1.32	-0.22	0.84	-0.02	-1.24	DARCI
$Pr(> Z)$	0.37	0.84	0.58	0.19	0.82	0.40	0.99	0.22	
ESS	1000.00	1160.17	1000.00	955.29	1000.00	1000.00	926.63	1000.00	
Z-score	0.48	-1.01	0.44	0.28	1.08	-2.18	-0.16	0.31	Reject
$Pr(> Z)$	0.63	0.31	0.66	0.78	0.28	0.03	0.87	0.76	
ESS	566.43	1000.00	1000.00	1000.00	538.12	907.14	729.33	1000.00	
Z-score	-1.25	-1.83	-0.48	-0.59	-2.09	-0.24	-1.52	-0.57	MH
$Pr(> Z)$	0.21	0.07	0.63	0.55	0.04	0.81	0.13	0.57	

We then compare “**DARCI**” and “**Reject**” in their running times (see Table 4). A dataset is simulated where there are different numbers of recoveries with unknown times within 5 time intervals. The two sampling methods are applied to draw a set of recovery times for each of those 5 intervals, and over multiple runs, the minimum and median times they take are recorded. Although the two methods draw samples from the same conditional distribution, “**DARCI**” tends to take less time than “**Reject**” in one iteration. Further results suggesting scalability to larger outbreaks are available in Supplement S5.

Table 4: Comparison between the two sampling methods (“**DARCI**” and “**Reject**”) for imputing missing recovery times. Overall, the DARCI algorithm is more efficient, especially when the number of missing recovery times is relatively large (e.g. Interval 3), or there are special constraints on viable recovery times (e.g. Interval 1, where the observed events suggest that the recovery cannot occur until half way through the time interval).

Interval	#(To recover)	Min Time		Median Time	
		Reject	DARCI	Reject	DARCI
1	1	227 μ s	224 μ s	484 μ s	245 μ s
2	8	285 μ s	287 μ s	563 μ s	319 μ s
3	15	163 μ s	161 μ s	279 μ s	181 μ s
4	2	138 μ s	138 μ s	153 μ s	156 μ s
5	1	133 μ s	133 μ s	146 μ s	147 μ s

6 Influenza-like-illnesses on a University Campus

In this section, we apply the proposed model and inference scheme to a real-world dataset on the transmission of influenza-like illnesses among students on a university campus.

6.1 Data Overview

The data we analyze in this section were collected in a 10-week network-based epidemiological study, eX-FLU (Aiello et al., 2016). The study was originally designed to investigate the effect of social intervention on respiratory infection transmission. 590 university students enrolled in the study and were asked to respond to weekly surveys on influenza-like illness (ILI) symptoms and social interactions. 103 individuals further participated in a sub-study in which each study subject was provided a smartphone equipped with an application, iEpi. The application pairs smartphones with other nearby study devices via Bluetooth, recording individual-level social interactions at five-minute intervals.

The sub-study using iEpi was carried out from January 28, 2013 to April 15, 2013 (from week 2 until after week 10). Between weeks 6 and 7, there was a one-week spring break

(March 1 to March 7), during which the volume of recorded social contacts dropped noticeably. In our experiments, we use data collected on the $N = 103$ sub-study participants from January 28 to April 4 (week 2 to week 10), and treat the two periods before and after the spring break as two separate and independent observation periods ($T_{\max} = 31$ days for period 1 and $T_{\max} = 28$ days for period 2).

Summary statistics of the data are provided in Table 5. Overall, infection instance counts peaked in the middle of each observation period and dropped at the end, and the dynamic social network was quite sparse; more activity (in both the epidemic process and network process) was observed in the weeks before the spring break. Further details on data cleaning and pre-processing are provided in Supplement S6.

Table 5: Summary statistics of the real data (processed) by week: number of new infection cases (top row), maximum network density (middle row), and minimum network density (bottom row). No new infection cases took place in week 2, but two participants were already ill at the beginning of the week. The dynamic network remained sparse throughout the duration of the sub-study, except for one instance in week 3—the unusually high network density only occurred on the night of February 4, possibly due to a large-scale on-campus social event.

Week	Wk 2	Wk 3	Wk 4	Wk 5	Wk 6
#(Infections)	0	3	5	4	2
Max. Density	0.0053	0.2048	0.0040	0.0038	0.0044
Min. Density	0.0000	0.0000	0.0000	0.0002	0.0000
Week	(break)	Wk 7	Wk 8	Wk 9	Wk 10
#(Infections)	N.A.	1	3	5	1
Max. Density	N.A.	0.0032	0.0032	0.0032	0.0023
Min. Density	N.A.	0.0000	0.0000	0.0000	0.0000

6.2 Analysis

Since the 103 individuals are sub-sampled from the 590 study participants, which are also sub-sampled from the university campus population, we treat the real data as observed on

an open population. Following the parametrization introduced at the end of Section 3.2, we include the parameter ξ to denote the rate of infection from an external source for each susceptible individual. Every infectious individual that came into contact with any infectives within 3 days prior to the onset of symptoms is regarded as an internal case (governed by parameter β); otherwise the infection is labeled as an external case (governed by parameter ξ). This enables the inference procedure stated at the end of Section 4.

The data collected during the two observation periods are considered as independent realizations of the same adaptive network epidemic processes. For each parameter, samples drawn in the first 500 iterations are discarded and then every other sample is retained in the next 2000 iterations, resulting in 1000 posterior samples. Table 6 summarizes the posterior sample means and the lower and upper bounds of 95% sample credible intervals for a selection of parameters. The output from one chain is presented here; repeated runs (with different initial conditions and random seeds) yield similar results.

The data provide symptom onset times for flu-like illnesses, which can serve as proxies for the actual infection times, but the former are on average 2 days later than the latter (US Centers for Disease Control & Prevention (CDC), 2018). To address this issue, we assume that the real infection times may be somewhere between 0 and 3 days prior to symptom onset (see Supplement S5.1) and thus randomly sample the latent infection times to generate multiple data versions for inference. Results are similar across different versions of data, suggesting that inference is robust to this choice of handling possible latency periods (this is summarized by the “Multi-SD” column of Table 6).

Our findings suggest that flu-like symptoms spread quite slowly but recoveries are made rather quickly. For instance, if a susceptible person maintains **one** infectious contact, then he has a probability of approximately 6.71% to contract infection through such contact **within one day**, and yet it takes (on average) a little more than 3 days for someone to no longer feel ill after infection. The external infection force is non-negligible: given the number of susceptibles in the population (typically about 100), the population-wide external infection rate is approximately $100 \times 0.0033 = 0.33$, implying that an external ILI case is expected to occur every other three days. This is a reasonable estimate consistent with having observed 9 external infection cases within 28 days during the second period.

Table 6: Posterior sample means and 95% credible intervals of select parameters (first 3 columns) obtained by the Bayesian inference scheme modified from that in Section 4. Inference is carried out jointly on the two periods before and after the spring break. The final column summarizes the standard deviations of posterior sample means across 10 versions of data, in which infection times are sampled randomly (and randomly) between 0 to 3 days prior to symptom onset.

Parameter	Posterior	2.5%	97.5%	Multi-SD
	Mean	Quantile	Quantile	
β (internal infection)	0.0695	0.0247	0.1500	0.0074
ξ (external infection)	0.00331	0.00208	0.00494	1.797×10^{-5}
γ (recovery)	0.294	0.186	0.428	0.0108
α_{SS} (S - S link activation)	0.0514	0.0499	0.0529	0.0002
ω_{SS} (S - S link termination)	38.26	33.55	40.62	0.2522
α_{SI} (S - I link activation)	0.130	0.0785	0.194	0.0097
ω_{SI} (S - I link termination)	53.5	22.5	231.7	31.4092

The inferred link rates reflect an interesting pattern in social interactions in this particular population: individuals are reluctant to establish contact and active contacts are broken off quickly—an average pair of healthy people initiate/restart their interaction after waiting 20 days and then end it after spending less than 40 minutes together. Moreover, it seems that on average a healthy-ill link is activated more frequently than a healthy-healthy link, but the former is also terminated faster—this might be because those students who fell ill in the duration of the study happen to be more socially proactive, but once their healthy social contacts realize they are sick and thus potentially infectious, the contact is cut short to avoid disease contraction.

It is also notable that the sample 95% credible intervals for β , α_{SI} and ω_{SI} are relatively wide, indicating a high level of uncertainty in the estimation for these parameters. It is challenging to estimate the internal infection rate β because dataset contains only 6 cases of internal infection in total (5 in period 1, 1 in period 2), providing limited information on the rate of transmission. Similar issues are present for the estimation of α_{SI} and ω_{SI} ; since there

were no more than 5 infectious individuals at any given time, network events related to them were few and far between. Moreover, since their exact recovery times are unknown, there is additional uncertainty associated with their exact disease statuses when they activated or terminated social links. Such measure of uncertainty, readily available through stochastic modeling and Bayesian inference, provides valuable insights into the amount of information the data contain and the level of confidence we possess when making conclusions and interpretations. The inference outcomes imply that, for example, the real data sufficiently inform the contact patterns among healthy individuals in this population but are limited toward understanding how long a healthy person and a symptomatic person typically maintain their contact.

7 Discussion

This paper has focused on enabling inference for partially observed epidemic processes on dynamic and adaptive networks. We formulated a continuous-time Markov process model to describe the epidemic-network interplay and derived its complete data likelihood. This leads to the design of conditional sampling techniques that enable data augmented inference methods to accommodate missingness in individual recovery times.

There are several limitations and natural extensions of our model. First, we address the issue of a latency period here by using a sensitivity analysis of the symptom onset time. As infectiousness is the focus of inference, we prefer this approach over, for instance, modeling an additional compartment (i.e. an SEIR model) in favor of model parsimony. We note that the latter is possible by extending our proposed likelihood framework, but introduces additional parameters that are often hard to identify without additional data directly informative of latency or modeling assumptions regarding the latency period (e.g., non-infectious or less infectious when latent).

A second extension of the model pertains to the handling of other missing data types. Motivated by our case study in which infection-related events (symptom onset) are updated daily, whereas recoveries are only provided at a much coarser resolution (in weekly summaries), our current method focuses on imputing missing recovery times.

While it is common in real-world data to focus on new cases (WHO, 2004, 2020), one may be provided with such incidence data at coarser time resolution so that infection times must also be imputed. Our framework applies in principle to such settings where missing infection times should be accounted for explicitly. One may derive analogous conditional samplers to DARCI, or at worst incur a computational tradeoff. Even without access to sampling from the exact conditional distributions, we can replace the Gibbs step to impute infection times by a Metropolis proposal within each iteration of the MCMC scheme (Britton and O’Neill, 2002).

Our contributions leverage network information to avoid a common model misspecification, but the current methods are limited to scenarios where such information is completely informed. If network dynamics are only partially observed—for instance link events are missing or exist only on a weekly survey basis—our proposed methods do not immediately apply, but can be extended via further data augmentation over unobserved network event times. Doing so falls under the same likelihood-based framework, yet practical challenges related to mixing of the Markov chain may arise due to the increased latent space. Another viable strategy is to adopt a discrete time model for network evolution that can be seen either as an alternative or an approximation to the link-Markovian jump process we propose. These directions remain open for future work.

We have demonstrated that accounting for changes in the contact structure is critical to accurately estimate disease parameters such as infection and recovery rates. Because our model is a generalization of existing compartmental models, such rates are consistent with their definitions and interpretation in existing literature. Other quantities such as the basic reproductive number R_0 , defined as the average number of infections caused by an infectious individual, do not translate as readily (Tunc et al., 2013; Van Segbroeck et al., 2010). This is the case when disease and network properties are conflated: the basic reproductive number depends on the product of infection rate β and number of contacts. The effect of interventions such as quarantine are often incorporated similarly, for instance by way of a change-point in β (Ho et al., 2018), yet such policies should naturally translate to changes in the contact network rather than the inherent infectivity of the disease. Because our model mechanistically describes the joint dynamics of the network and the disease spread, such

phenomena can now be modeled explicitly in terms of network parameters rather than indirectly through disease parameters, leading to more accurate and interpretable inference. The proposed framework thus serves as a point of departure to further explore these promising extensions.

SUPPLEMENTARY MATERIAL

Supplementary information: Supplementary proofs and derivations, inference details on open population epidemics, and more results from simulation experiments and real data experiments. (.pdf file: `supplement.pdf`)

Codes and examples: R codes for all simulation experiments, accompanied by example synthetic datasets. (Anonymized repository: <https://anonymous.4open.science/r/2231b6ae-00aa-414c-9d6f-37c69084e5a0/>)

References

- Aiello, A. E., A. M. Simanek, M. C. Eisenberg, A. R. Walsh, B. Davis, E. Volz, C. Cheng, J. J. Rainey, A. Uzicanin, H. Gao, et al. (2016). Design and methods of a social network isolation study for reducing respiratory infection transmission: The eX-FLU cluster randomized trial. *Epidemics* 15, 38–55.
- Anderson, R. M. and R. M. May (1992). *Infectious diseases of humans: dynamics and control*. Oxford university press.
- Andrieu, C., A. Doucet, and R. Holenstein (2010). Particle Markov chain Monte Carlo methods. *Journal of the Royal Statistical Society: Series B (Statistical Methodology)* 72(3), 269–342.
- Auranen, K., E. Arjas, T. Leino, and A. K. Takala (2000). Transmission of pneumococcal carriage in families: a latent Markov process model for binary longitudinal data. *Journal of the American Statistical Association* 95(452), 1044–1053.

- Bailey, N. T. et al. (1975). *The mathematical theory of infectious diseases and its applications*. Number 2nd edition. Charles Griffin & Company Ltd 5a Crendon Street, High Wycombe, Bucks HP13 6LE.
- Barabási, A.-L. and R. Albert (1999). Emergence of scaling in random networks. *science* 286(5439), 509–512.
- Barrat, A., C. Cattuto, A. E. Tozzi, P. Vanhems, and N. Voirin (2014). Measuring contact patterns with wearable sensors: methods, data characteristics and applications to data-driven simulations of infectious diseases. *Clinical Microbiology and Infection* 20(1), 10–16.
- Becker, N. G. and T. Britton (1999). Statistical studies of infectious disease incidence. *Journal of the Royal Statistical Society: Series B (Statistical Methodology)* 61(2), 287–307.
- Bell, D., A. Nicoll, K. Fukuda, P. Horby, and A. Monto (2006). World health organization writing group. non-pharmaceutical interventions for pandemic influenza, national and community measures. *Emerg Infect Dis* 12(1), 88–94.
- Britton, T. (2010). Stochastic epidemic models: a survey. *Mathematical biosciences* 225(1), 24–35.
- Britton, T. (2020). Epidemic models on social networks—with inference. *Statistica Neerlandica*.
- Britton, T. and P. D. O’Neill (2002). Bayesian inference for stochastic epidemics in populations with random social structure. *Scandinavian Journal of Statistics* 29(3), 375–390.
- Cauchemez, S. and N. M. Ferguson (2008). Likelihood-based estimation of continuous-time epidemic models from time-series data: application to measles transmission in london. *Journal of the Royal Society Interface* 5(25), 885–897.
- Cauchemez, S., L. Temime, A.-J. Valleron, E. Varon, G. Thomas, D. Guillemot, and P.-Y. Boëlle (2006). S. pneumoniae transmission according to inclusion in conjugate vaccines:

- Bayesian analysis of a longitudinal follow-up in schools. *BMC Infectious Diseases* 6(1), 14.
- Clementi, A. E., C. Macci, A. Monti, F. Pasquale, and R. Silvestri (2010). Flooding time of edge-Markovian evolving graphs. *SIAM journal on discrete mathematics* 24(4), 1694–1712.
- Dong, W., A. Pentland, and K. A. Heller (2012). Graph-coupled hmms for modeling the spread of infection. *arXiv preprint arXiv:1210.4864*.
- Eames, K., N. Tilston, P. White, E. Adams, and W. Edmunds (2010). The impact of illness and the impact of school closure on social contact patterns. *Health technology assessment (Winchester, England)* 14(34), 267–312.
- Edmunds, W., G. Kafatos, J. Wallinga, and J. Mossong (2006). Mixing patterns and the spread of close-contact infectious diseases. *Emerging themes in epidemiology* 3(1), 10.
- Edmunds, W. J., C. O’callaghan, and D. Nokes (1997). Who mixes with whom? A method to determine the contact patterns of adults that may lead to the spread of airborne infections. *Proceedings of the Royal Society of London. Series B: Biological Sciences* 264(1384), 949–957.
- Fan, K., M. Eisenberg, A. Walsh, A. Aiello, and K. Heller (2015). Hierarchical graph-coupled hmms for heterogeneous personalized health data. In *Proceedings of the 21th ACM SIGKDD international conference on knowledge discovery and data mining*, pp. 239–248. ACM.
- Fan, K., C. Li, and K. Heller (2016). A unifying variational inference framework for hierarchical graph-coupled hmm with an application to influenza infection. In *Thirtieth AAAI Conference on Artificial Intelligence*.
- Ferguson, N. M., D. Laydon, G. Nedjati-Gilani, and et al. (2020). Impact of non-pharmaceutical interventions (npis) to reduce covid19 mortality and healthcare demand. *Imperial College COVID-19 Response Team*.

- Fintzi, J., X. Cui, J. Wakefield, and V. N. Minin (2017). Efficient data augmentation for fitting stochastic epidemic models to prevalence data. *Journal of Computational and Graphical Statistics* 26(4), 918–929.
- Funk, S., M. Salathé, and V. A. Jansen (2010). Modelling the influence of human behaviour on the spread of infectious diseases: a review. *Journal of the Royal Society Interface* 7(50), 1247–1256.
- Geweke, J. et al. (1991). *Evaluating the accuracy of sampling-based approaches to the calculation of posterior moments*, Volume 196. Federal Reserve Bank of Minneapolis, Research Department Minneapolis, MN.
- Gillespie, D. T. (1976). A general method for numerically simulating the stochastic time evolution of coupled chemical reactions. *Journal of computational physics* 22(4), 403–434.
- Guttorp, P. and V. N. Minin (2018). *Stochastic modeling of scientific data*. Chapman and Hall/CRC.
- He, D., E. L. Ionides, and A. A. King (2010). Plug-and-play inference for disease dynamics: measles in large and small populations as a case study. *Journal of the Royal Society Interface* 7(43), 271–283.
- Hethcote, H. W. (2000). The mathematics of infectious diseases. *SIAM review* 42(4), 599–653.
- Ho, L. S. T., F. W. Crawford, M. A. Suchard, et al. (2018). Direct likelihood-based inference for discretely observed stochastic compartmental models of infectious disease. *The Annals of Applied Statistics* 12(3), 1993–2021.
- Ho, L. S. T., J. Xu, F. W. Crawford, V. N. Minin, and M. A. Suchard (2018). Birth/birth-death processes and their computable transition probabilities with biological applications. *Journal of Mathematical Biology* 76(4), 911–944.
- Hobolth, A. and E. A. Stone (2009). Simulation from endpoint-conditioned, continuous-time Markov chains on a finite state space, with applications to molecular evolution. *The Annals of Applied Statistics* 3(3), 1204.

- Höhle, M. and E. Jørgensen (2002). *Estimating parameters for stochastic epidemics*. [The Royal Veterinary and Agricultural University], Dina.
- Hoti, F., P. Erästö, T. Leino, and K. Auranen (2009). Outbreaks of streptococcus pneumoniae carriage in day care cohorts in finland—implications for elimination of transmission. *BMC infectious diseases* 9(1), 102.
- Kermack, W. O. and A. G. McKendrick (1927). A contribution to the mathematical theory of epidemics. *Proceedings of the royal society of london. Series A, Containing papers of a mathematical and physical character* 115(772), 700–721.
- Kiss, I. Z., L. Berthouze, T. J. Taylor, and P. L. Simon (2012). Modelling approaches for simple dynamic networks and applications to disease transmission models. *Proceedings of the Royal Society A: Mathematical, Physical and Engineering Sciences* 468(2141), 1332–1355.
- Kiti, M. C., M. Tizzoni, T. M. Kinyanjui, D. C. Koech, P. K. Munywoki, M. Meriac, L. Cappa, A. Panisson, A. Barrat, C. Cattuto, et al. (2016). Quantifying social contacts in a household setting of rural Kenya using wearable proximity sensors. *EPJ Data Science* 5(1), 21.
- Korea Centers for Disease Control & Prevention (2020). The updates on COVID-19 in Korea. <https://www.cdc.go.kr/board/board.es?mid=a30402000000&bid=0030>. Public Press Release.
- Masuda, N. and P. Holme (2017). *Temporal network epidemiology*. Springer.
- Melegaro, A., M. Jit, N. Gay, E. Zagheni, and W. J. Edmunds (2011). What types of contacts are important for the spread of infections? Using contact survey data to explore European mixing patterns. *Epidemics* 3(3-4), 143–151.
- Ministry Of Health, State of Israel (2020). Press releases. https://www.health.gov.il/English/News_and_Events/Spokespersons_Messages/Pages/default.aspx. Public Resource of Israel Case Information.

- Mossong, J., N. Hens, M. Jit, P. Beutels, K. Auranen, R. Mikolajczyk, M. Massari, S. Salmaso, G. S. Tomba, J. Wallinga, et al. (2008). Social contacts and mixing patterns relevant to the spread of infectious diseases. *PLoS medicine* 5(3), e74.
- Neal, P. J. and G. O. Roberts (2004). Statistical inference and model selection for the 1861 Hagelloch measles epidemic. *Biostatistics* 5(2), 249–261.
- Ogura, M. and V. M. Preciado (2016). Stability of spreading processes over time-varying large-scale networks. *IEEE Transactions on Network Science and Engineering* 3(1), 44–57.
- Ogura, M. and V. M. Preciado (2017). Optimal containment of epidemics in temporal and adaptive networks. In *Temporal Network Epidemiology*, pp. 241–266. Springer.
- O’Neill, P. D. (2009). Bayesian inference for stochastic multitype epidemics in structured populations using sample data. *Biostatistics* 10(4), 779–791.
- Ozella, L., F. Gesualdo, M. Tizzoni, C. Rizzo, E. Pandolfi, I. Campagna, A. E. Tozzi, and C. Cattuto (2018). Close encounters between infants and household members measured through wearable proximity sensors. *PloS one* 13(6), e0198733.
- Pooley, C., S. Bishop, and G. Marion (2015). Using model-based proposals for fast parameter inference on discrete state space, continuous-time Markov processes. *Journal of The Royal Society Interface* 12(107), 20150225.
- Shaw, L. B. and I. B. Schwartz (2008). Fluctuating epidemics on adaptive networks. *Physical Review E* 77(6), 066101.
- Tsang, T. K., V. J. Fang, D. K. M. Ip, R. A. P. M. Perera, H. C. So, G. M. Leung, J. S. M. Peiris, B. J. Cowling, and S. Cauchemez (2019). Indirect protection from vaccinating children against influenza in households. *Nature Communications* 10(1), 106.
- Tunc, I., M. S. Shkarayev, and L. B. Shaw (2013). Epidemics in adaptive social networks with temporary link deactivation. *Journal of statistical physics* 151(1-2), 355–366.
- US Centers for Disease Control & Prevention (CDC) (2018). Key facts about influenza (flu). <https://www.cdc.gov/flu/about/keyfacts.htm>.

- Van Kerckhove, K., N. Hens, W. J. Edmunds, and K. T. Eames (2013). The impact of illness on social networks: implications for transmission and control of influenza. *American journal of epidemiology* 178(11), 1655–1662.
- Van Segbroeck, S., F. C. Santos, and J. M. Pacheco (2010). Adaptive contact networks change effective disease infectiousness and dynamics. *PLoS computational biology* 6(8), e1000895.
- Vanhems, P., A. Barrat, C. Cattuto, J.-F. Pinton, N. Khanafer, C. Régis, B.-a. Kim, B. Comte, and N. Voirin (2013). Estimating potential infection transmission routes in hospital wards using wearable proximity sensors. *PloS one* 8(9), e73970.
- Voirin, N., C. Payet, A. Barrat, C. Cattuto, N. Khanafer, C. Régis, B.-a. Kim, B. Comte, J.-S. Casalegno, B. Lina, and P. Vanhems (2015). Combining high-resolution contact data with virological data to investigate influenza transmission in a tertiary care hospital. *Infection Control & Hospital Epidemiology* 36, 254.
- Volz, E. (2008). SIR dynamics in random networks with heterogeneous connectivity. *Journal of mathematical biology* 56(3), 293–310.
- Volz, E. and L. A. Meyers (2007). Susceptible–infected–recovered epidemics in dynamic contact networks. *Proceedings of the Royal Society B: Biological Sciences* 274(1628), 2925–2934.
- Volz, E. and L. A. Meyers (2008). Epidemic thresholds in dynamic contact networks. *Journal of the Royal Society Interface* 6(32), 233–241.
- Wallinga, J., W. J. Edmunds, and M. Kretzschmar (1999). Perspective: human contact patterns and the spread of airborne infectious diseases. *TRENDS in Microbiology* 7(9), 372–377.
- WHO (2004). Cumulative number of reported probable cases of severe acute respiratory syndrome (SARS). <https://www.who.int/csr/sars/country/en/>.

WHO (2020). Coronavirus disease (COVID-2019) situation reports. <https://www.who.int/emergencies/diseases/novel-coronavirus-2019/situation-report>.

WHOW Group (2006). Nonpharmaceutical interventions for pandemic influenza, national and community measures. *Emerging infectious diseases* 12(1), 88.

Yang, C. H. and H. Jung (2020). Topological dynamics of the 2015 south korea mers-cov spread-on-contact networks. *Scientific Reports* 10(1), 4327.

SUPPLEMENTARY INFORMATION

S1 Complete Data Likelihood for SIS-type Contagions

Here we consider an SIS-type infectious disease to illustrate how our methodology can be applied to similar model classes. The complete data likelihood can be derived following the same steps in Section 3.2. Alternatively, one can slightly modify (14) to arrive at the complete likelihood for an SIS-type contagion. Since an individual doesn't acquire immunity upon recovery, it is equivalent to setting $H(t) \equiv S(t)$ at any time t . Thus the complete data likelihood is

$$\begin{aligned} & \mathcal{L}(\beta, \gamma, \tilde{\alpha}, \tilde{\omega} | \mathcal{G}_0) \\ &= \gamma^{n_R} \beta^{n_E - 1} \alpha_{SS}^{C_{SS}} \alpha_{SI}^{C_{SI}} \alpha_{II}^{C_{II}} \omega_{SS}^{D_{SS}} \omega_{SI}^{D_{SI}} \omega_{II}^{D_{II}} \prod_{j=2}^n \left[\tilde{M}(t_j) (I_{p_{j1}}(t_j))^{F_j} \right] \\ & \times \exp \left(- \int_0^{T_{\max}} [\beta SI(t) + \gamma I(t) + \tilde{\alpha}^T \mathbf{M}_{\max}(t) + (\tilde{\omega} - \tilde{\alpha})^T \mathbf{M}(t)] dt \right). \end{aligned} \quad (20)$$

S2 Auxiliary Proofs and Derivations

Proof for Theorem 3.1 From (14), we can obtain the log-likelihood:

$$\begin{aligned} \ell(\beta, \gamma, \tilde{\alpha}, \tilde{\omega} | \mathcal{G}_0) &= \log \mathcal{L}(\beta, \gamma, \tilde{\alpha}, \tilde{\omega} | \mathcal{G}_0) \\ &= \sum_{j=2}^n \left[\log \tilde{M}(t_j) + F_j \log (I_{p_{j1}}(t_j)) \right] + n_R \log \gamma + (n_E - 1) \log \beta \\ & \quad + C_{HH} \log \alpha_{SS} + C_{HI} \log \alpha_{SI} + C_{II} \log \alpha_{II} + D_{HH} \log \omega_{SS} + D_{HI} \log \omega_{SI} + D_{II} \log \omega_{II} \\ & \quad - \sum_{j=1}^n [\beta SI(t_j) + \gamma I(t_j) + \tilde{\alpha}^T (\mathbf{M}_{\max}(t_j) - \mathbf{M}(t_j)) + \tilde{\omega}^T \mathbf{M}(t_j)] (t_j - t_{j-1}). \end{aligned} \quad (21)$$

Taking partial derivatives of the right hand side of (21) with respect to the parameters and setting them to zero yield the results above.

S3 Relaxing the Closed Population Assumption

Suppose the observed population is not fully closed, but is a subset of a larger yet unobserved population. Then it is possible for an individual to get infected by an outsider. Let ξ be the “external infection” rate, the rate for any susceptible individual to be infected by any external infectious source, then the complete data likelihood is

$$\begin{aligned} \mathcal{L}(\beta, \xi, \gamma, \tilde{\alpha}, \tilde{\omega} | \mathcal{G}_0) &= p(\text{epidemic events, network events} | \beta, \xi, \gamma, \alpha, \omega, \mathcal{G}_0) \\ &= \gamma^{n_R} \alpha_{SS}^{C_{HH}} \alpha_{SI}^{C_{HI}} \alpha_{II}^{C_{II}} \omega_{SS}^{D_{HH}} \omega_{SI}^{D_{HI}} \omega_{II}^{D_{II}} \prod_{j=2}^n \left[\tilde{M}(t_j) (\beta I_{p_{j1}}(t_j) + \xi)^{F_j} \right] \\ &\quad \times \exp \left(- \int_0^{T_{\max}} [\beta SI(t) + \xi S(t) + \gamma I(t) + \tilde{\alpha}^T \mathbf{M}_{\max}(t) + (\tilde{\omega} - \tilde{\alpha})^T \mathbf{M}(t)] dt \right). \end{aligned} \quad (22)$$

MLEs for $\{\gamma, \tilde{\alpha}, \tilde{\omega}\}$ remain unchanged, but estimating β and ξ is less straightforward. Let $\ell(\beta, \xi, \gamma, \tilde{\alpha}, \tilde{\omega} | \mathcal{G}_0)$ be the log-likelihood, then the partial derivatives of the log-likelihood w.r.t. β and ξ are

$$\begin{aligned} \frac{\partial \ell}{\partial \beta} &= \sum_{j=2}^n \frac{F_j I_{p_{j1}}(t_j)}{\beta I_{p_{j1}}(t_j) + \xi} - \sum_{j=1}^n SI(t_j)(t_j - t_{j-1}), \\ \frac{\partial \ell}{\partial \xi} &= \sum_{j=2}^n \frac{F_j}{\beta I_{p_{j1}}(t_j) + \xi} - \sum_{j=1}^n S(t_j)(t_j - t_{j-1}), \end{aligned}$$

which do not directly lead to closed-form solutions.

Reparameterizing by $\xi = \kappa\beta$ leads to the following partially derivatives

$$\frac{\partial \ell}{\partial \beta} = \frac{n_E - 1}{\beta} - \sum_{j=1}^n [SI(t_j) + \kappa S(t_j)](t_j - t_{j-1}), \quad (23)$$

$$\frac{\partial \ell}{\partial \kappa} = \sum_{j=2}^n \frac{F_j}{I_{p_{j1}}(t_j) + \kappa} - \beta \sum_{j=1}^n S(t_j)(t_j - t_{j-1}), \quad (24)$$

which are slightly more straightforward in form, and can be solved numerically to obtain the MLEs.

If, somehow, we have information on which infection cases are caused by internal sources and which are caused by external sources, then we can directly obtain the MLEs and Bayesian posterior distributions for all the parameters. For an infection event e_j (with $F_j = 1$), let $\text{Int}_j = 1$ if it is “internal” and let $\text{Int}_j = 0$ otherwise. Then the complete data likelihood can

be re-written as

$$\begin{aligned}
& \mathcal{L}(\beta, \xi, \gamma, \tilde{\alpha}, \tilde{\omega} | \mathcal{G}_0) \\
&= \beta^{(n_E^{\text{int}} - \text{Int}_1)} \xi^{(n_E^{\text{ext}} - 1 + \text{Int}_1)} \gamma^{n_R} \alpha_{SS}^{C_{HH}} \alpha_{SI}^{C_{HI}} \alpha_{II}^{C_{II}} \omega_{SS}^{D_{HH}} \omega_{SI}^{D_{HI}} \omega_{II}^{D_{II}} \prod_{j=2}^n \left[\tilde{M}(t_j) I_{p_{j1}}(t_j)^{F_j \text{Int}_j} \right] \\
& \times \exp \left(- \int_0^{T_{\max}} [\beta SI(t) + \xi S(t) + \gamma I(t) + \tilde{\alpha}^T \mathbf{M}_{\max}(t) + (\tilde{\omega} - \tilde{\alpha})^T \mathbf{M}(t)] dt \right), \quad (25)
\end{aligned}$$

where n_E^{int} and n_E^{ext} are the total numbers of internal and external infection events, respectively.

Estimation for all parameters remains unchanged except for β and ξ . Their MLEs are

$$\hat{\beta} = \frac{n_E^{\text{int}} - \text{Int}_1}{\sum_{j=1}^n SI(t_j)(t_j - t_{j-1})}, \quad \hat{\xi} = \frac{n_E^{\text{ext}} - 1 + \text{Int}_1}{\sum_{j=1}^n S(t_j)(t_j - t_{j-1})}, \quad (26)$$

and with Gamma priors $\beta \sim Ga(a_\beta, b_\beta)$ and $\xi \sim Ga(a_\xi, b_\xi)$, their posterior distributions are

$$\beta | \{e_j\} \sim Ga \left(a_\beta + (n_E^{\text{int}} - \text{Int}_1), b_\beta + \sum_{j=1}^n SI(t_j)(t_j - t_{j-1}) \right), \quad (27)$$

$$\xi | \{e_j\} \sim Ga \left(a_\xi + (n_E^{\text{ext}} - 1 + \text{Int}_1), b_\xi + \sum_{j=1}^n S(t_j)(t_j - t_{j-1}) \right). \quad (28)$$

When there is missingness in recovery times, the Bayesian inference procedure described in Section 4 can still be carried out, with two slight modifications. First, in the data augmentation step, when drawing missing recovery times in an interval $(u, v]$, the DARCI algorithm (Prop. 4.2) inspects \mathcal{I}_p only for each $p \in \mathcal{P}^{\text{int}}$, where \mathcal{P}^{int} is the group of individuals who get *internally* infected during $(u, v]$. Second, in each iteration, parameter values are drawn from the posterior distributions specified in (15) except for β and ξ , for which the posteriors are stated in (27) and (28), respectively.

S4 Flexible Network Dynamics under the Generative Model

As stated in the main text, the proposed generative model can accommodate **arbitrary** initial network structures. Moreover, due to the **coupled** nature of the epidemic process and

the network process, different choices of parameters can lead to a wide variety of network behaviors.

Here we demonstrate via simulations that, even if the initial network follows a simple, idealized model, it can still evolve and adapt to exhibit characteristics that are no longer simple and idealistic throughout the process.

Setting the population size to $N = 500$, we assume two different models for the initial network: 1) a random Erdős–Rényi graph (“ER”), and 2) a random **scale-free** network (sampled using the Barabasi-Albert model (“BA”) (Barabási and Albert, 1999)). The “ER” model leads to a degree distribution close to Poisson, whereas the “BA” model leads to power-law degree distribution.

Using the following parameter settings (same as those in most of our simulations),

$$\begin{aligned}\beta &= 0.03, \gamma = 0.12; \\ \tilde{\alpha}^T &= (\alpha_{SS}, \alpha_{SI}, \alpha_{II}) = (0.005, 0.001, 0.005), \\ \tilde{\omega}^T &= (\omega_{SS}, \omega_{SI}, \omega_{II}) = (0.05, 0.1, 0.05).\end{aligned}$$

we adopt a dynamic that 1) discourages new $S - I$ connections and thus effectively “isolates” super-spreaders probabilistically, and 2) mostly sustains the usual contact activities between $S - S$, $R - R$ and $I - I$ pairs. This, during the process, can lead to a **bi-modal** degree distribution that obviously deviates from the initial degree distribution.

Below in Figure S1, we include the empirical degree distributions at the start and the end of a typical simulation, with a random Erdős–Rényi graph as the initial network. Here the red curve represents the actual degree distribution in the simulated population, and (in contrast) the lightblue curve represents the density of a degree sequence sampled from a Poisson with the same mean degree.

For comparison, in Figure S2 we include similar plots with the initial network as a **scale-free** network (sampled using the Barabasi-Albert model). Note that the initial network setting here is similar to that used in Volz and Meyers (2007), but our dynamic network model is fundamentally different from (and more flexible) than the neighbor-exchange framework proposed in that work.

We can observe that, once the network dynamics kicks in, the initial network struc-

ture doesn't matter that much, as changes in the network links are driven jointly by the parameters and the epidemic dynamics in time.

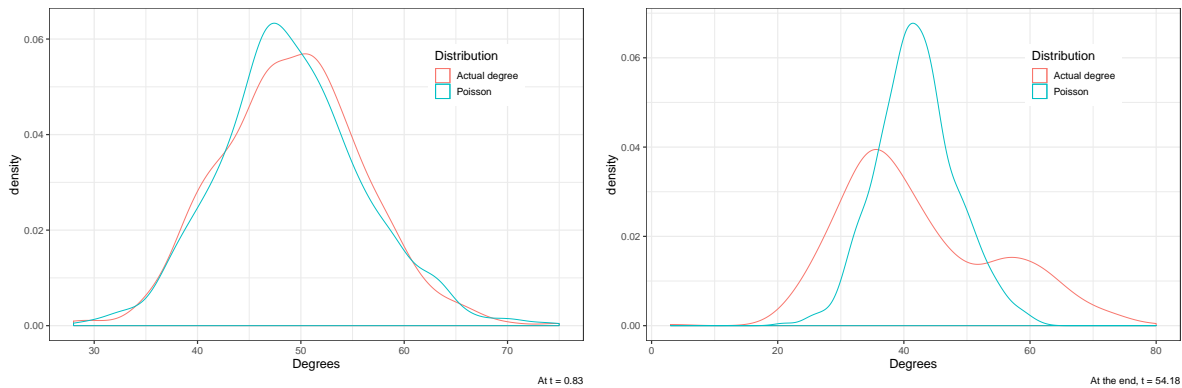


Figure S1: Actual empirical degree distribution in simulation (red) versus empirical degree distribution drawn from Poisson (blue/green). Here the initial network is a random Erdős–Rényi graph. **Left: beginning of process; right: end of process.**

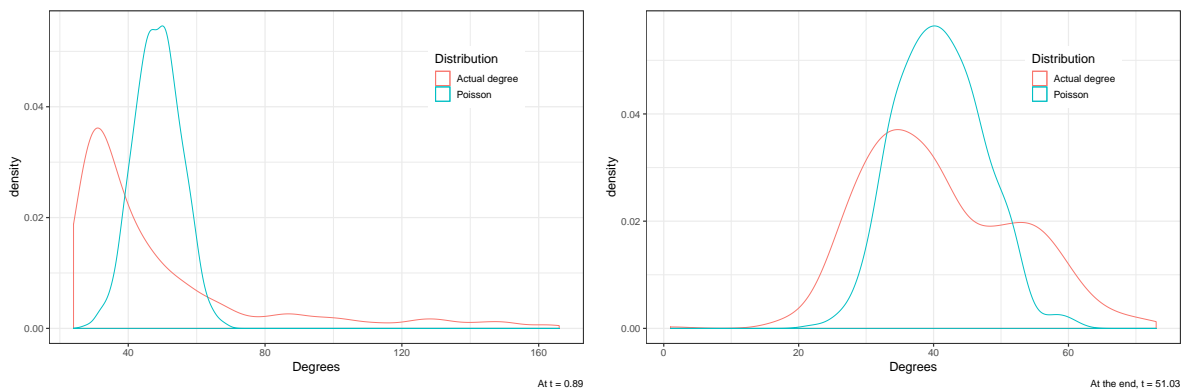


Figure S2: Actual empirical degree distribution in simulation (red) versus empirical degree distribution drawn from Poisson (blue/green). Here the initial network is a random scale-free network (sampled using the Barabasi-Albert model (Barabási and Albert, 1999)). **Left: beginning of process; right: end of process.**

S5 More Results on Simulation Experiments

Supplement for “inference from complete event data” Figure S3 and S4 complement Figure 2 and 3 in the main text, showing inference results for all the parameters in the

corresponding experiments.

Experiments on larger networks Figure S5 shows MLEs and 95% confidence bands for parameters with complete data generated on a network with $N = 500$ individuals. Other experimental settings are the same as those in Section 5.1. With a larger population, there tends to be more events available for inference, so the accuracy is in fact improved.

Experiments on different initial network configurations Still set population size $N = 100$, but instead of a random Erdős–Rényi graph as \mathcal{G}_0 , the initial network is a “hubnet”: one individual (the “hub”) is connected to everyone else in the population while the others form an $ER(N - 1, p)$ random graph, with edge probability $p = 0.1$. Figure S6 summarizes results of Bayesian inference carried out on complete event data generated in this setting.

Supplement for “Assessing model flexibility” Estimate parameters Θ of the full model on datasets generated from 1) the decoupled temporal network epidemic process with type-independent edge rates, and 2) the static network epidemic process where the network remains unchanged. For both simpler models, fix $\beta = 0.03$ and $\gamma = 0.12$, and for the former model, let link activation rate $\alpha = 0.005$ and termination rate $\omega = 0.05$. Still, set population size $N = 100$ and let the initial network be a random Erdős–Rényi graph with edge probability $p = 0.1$.

We present, in Figure S7, the results of Bayesian inference on datasets generated from the decoupled process model. Across four different realizations, it can be observed that, the posterior samples of link activation rates $(\alpha_{SS}, \alpha_{SI}, \alpha_{II})$ concentrate around the same mean, and uncertainty is reduced with more events available for inference. Same can be said about the link termination rates, $\omega_{SS}, \omega_{SI}, \omega_{II}$. This verifies that the proposed model is indeed a generalization of the aforementioned two simpler processes, and the inference method is able to recover the truth under mild model misspecification.

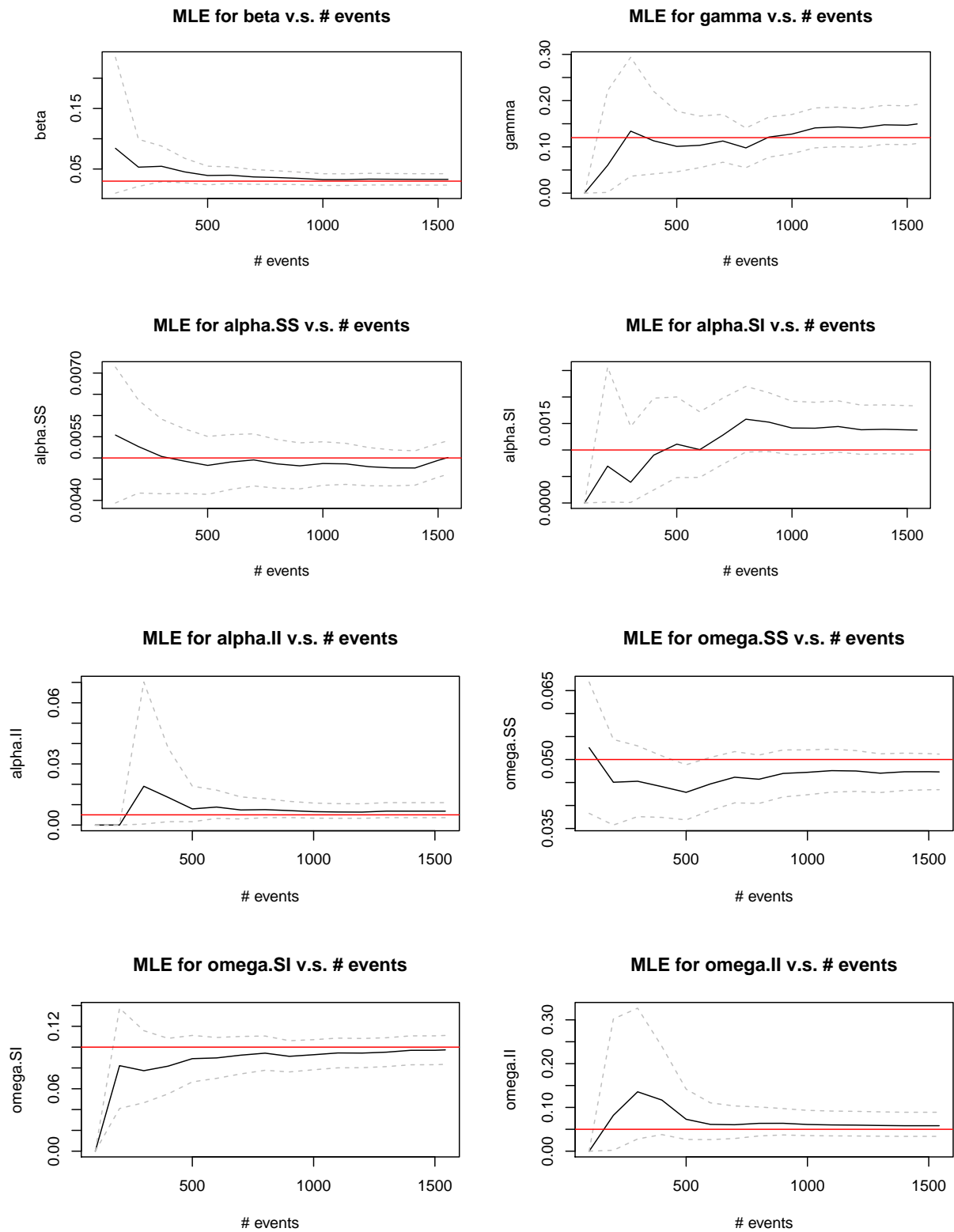


Figure S3: MLEs versus number of events used for inference. Dashed gray lines show the lower and upper bounds for 95% frequentist confidence intervals, and red lines mark the true parameter values.

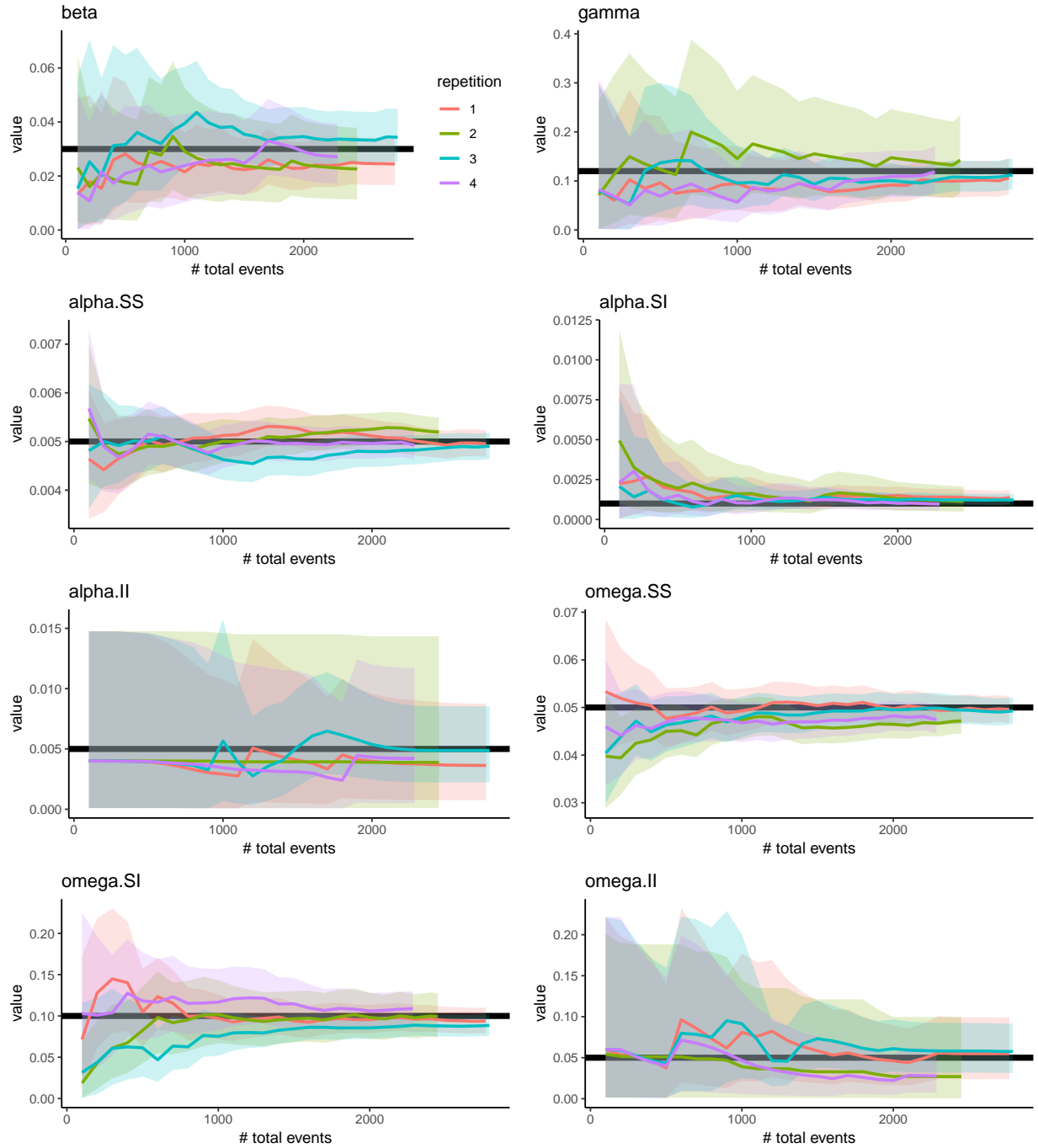


Figure S4: Posterior sample means v.s. number of total events used for inference. True parameter values are marked by **bold dark** horizontal lines, along with 95% credible bands. Results are presented for 4 different complete datasets.

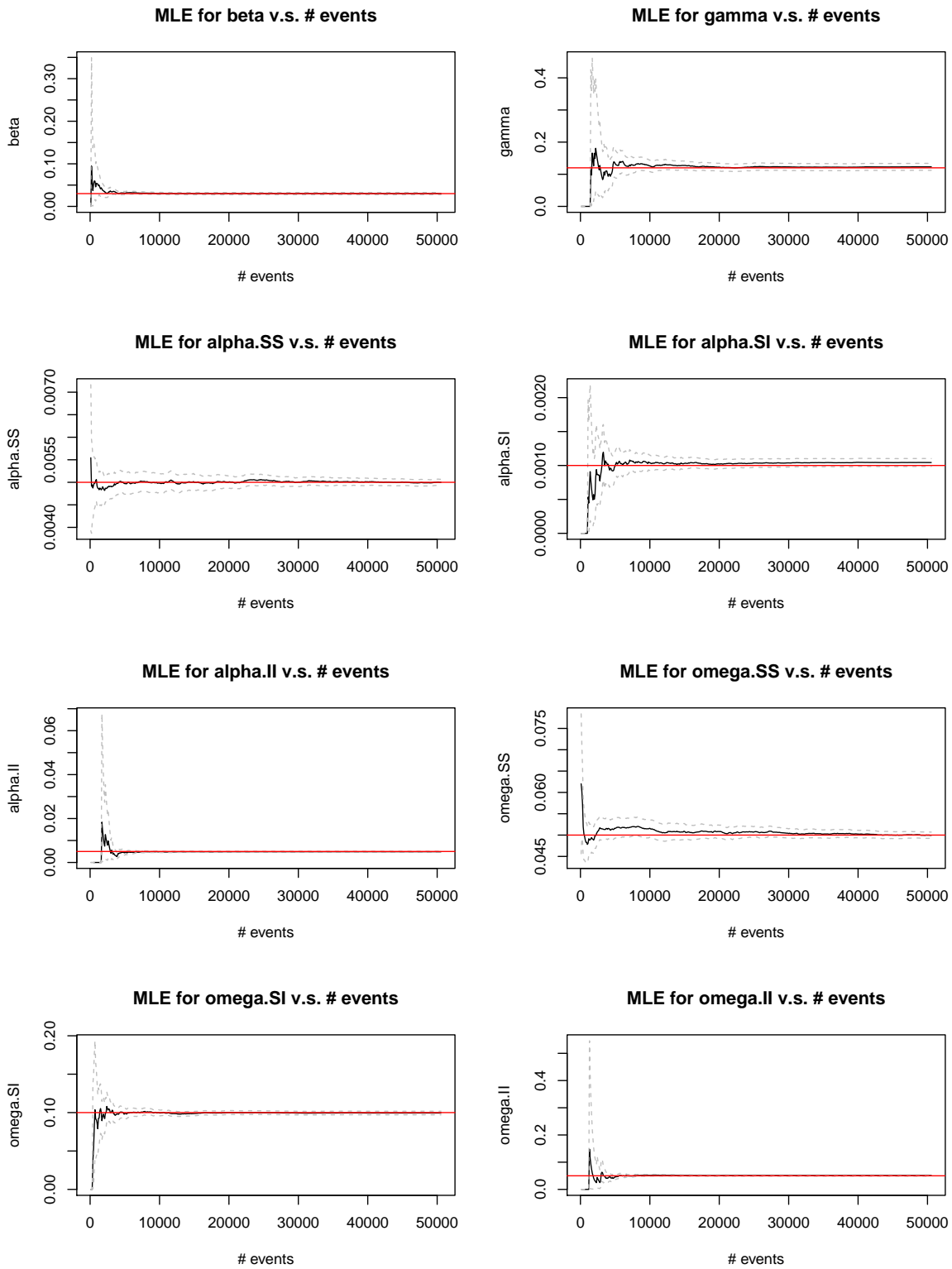


Figure S5: MLEs versus number of total events, on a larger population with $N = 500$. Dashed gray lines show the lower and upper bounds for 95% confidence intervals, and red lines mark the true parameter values. With a larger population size, there tends to be more events, which in fact facilitates estimation.

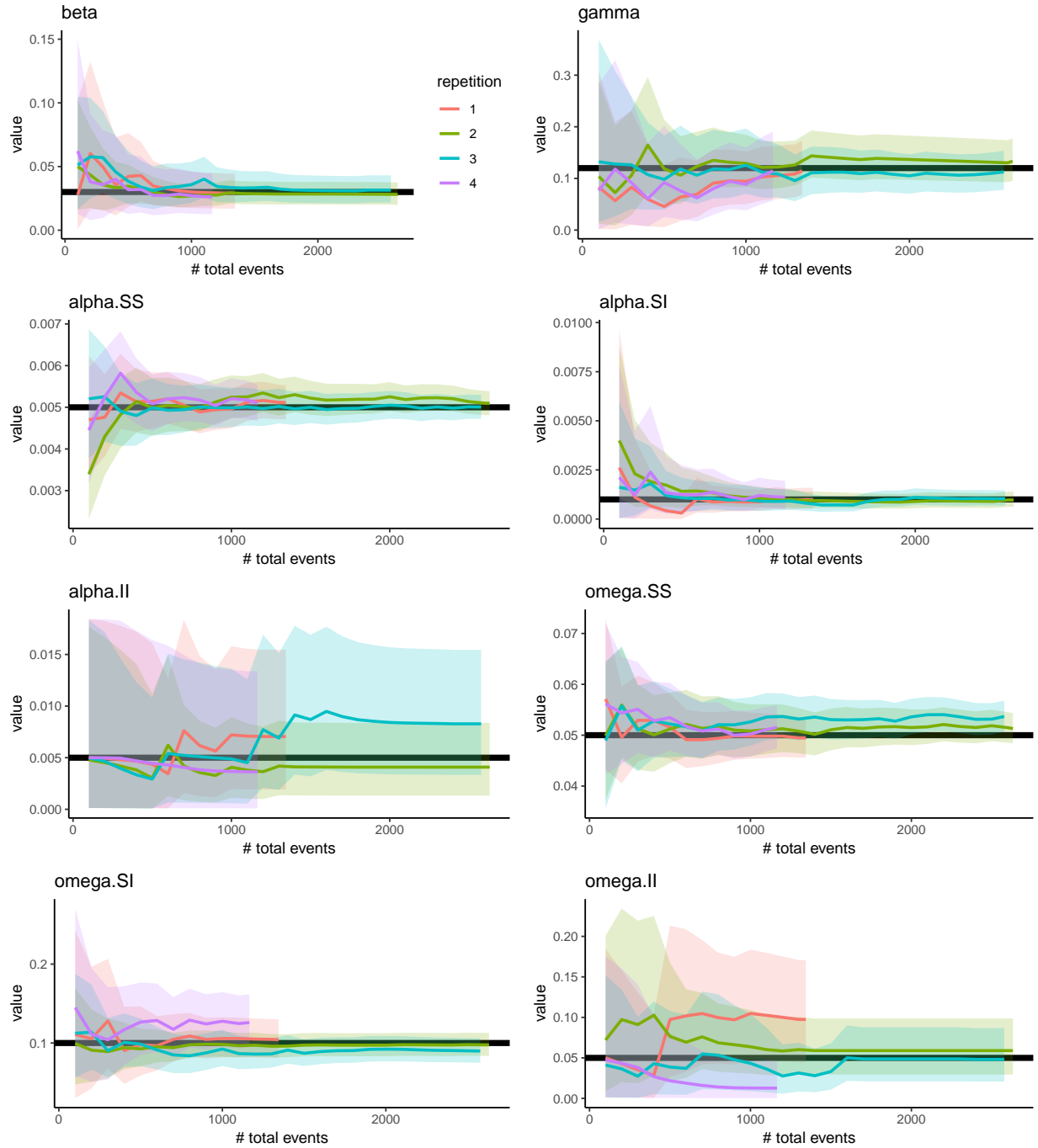


Figure S6: Posterior sample means v.s. number of total events, with \mathcal{G}_0 as a $N = 100$ -node “hubnet”. True parameter values are marked by **bold dark** horizontal lines, along with 95% credible bands. Results are presented for 4 different complete datasets.

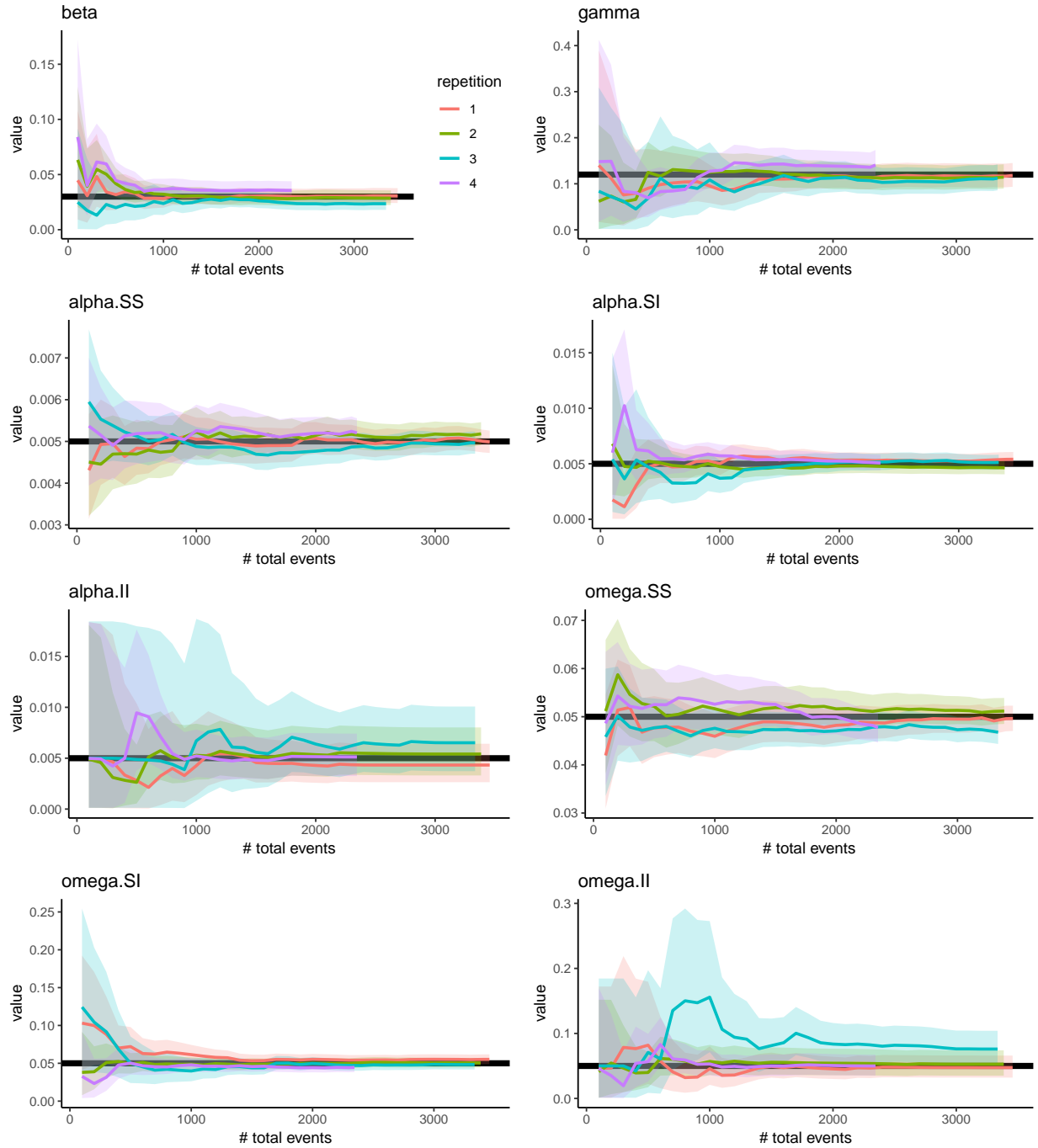


Figure S7: Posterior sample means versus number of total events, estimated using datasets generated by the decoupled process model. True parameter values are marked by **bold dark** horizontal lines, along with 95% credible bands. Results are presented for 4 different complete datasets.

Scalability of DARCI and the data-augmented inference scheme In the main text, most simulations are conducted on a population of size $N = 100$, in order to mimic the

population size of the real data, but experiments have been carried out on larger networks (for example, with $N = 200$ and $N = 500$). Here we include some inference results for $N = 500$ (see Figure S8).

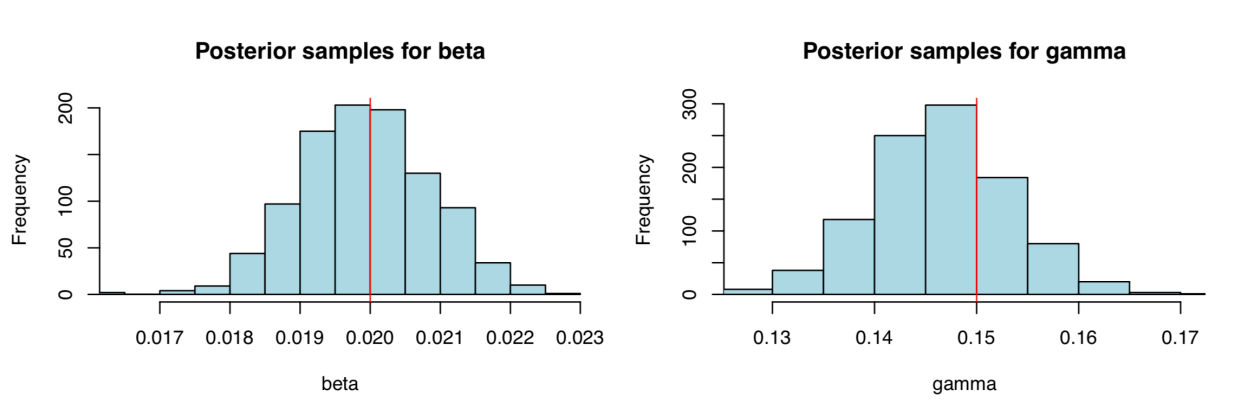


Figure S8: Inference performance with population size $N = 500$. Here we show histograms of posterior samples for parameter β (infection rate, left panel) and γ (recovery rate, right panel); ground truth is represented by red vertical lines. The proposed inference scheme can certainly handle a relatively large population with a lot of events, and can recover parameter values accurately.

It seems that the inference scheme is effective in recovering parameters and is capable of handling a large population and many events. Our finding is that computing time scales linearly with the total number of events observed. Figure S9 shows the computing time on a single processor for each iteration with population size $N = 500$, using a naive implementation in R. Since DARCI is parallelizable across time intervals, a more efficient implementation can further reduce computing time, and the algorithm bottleneck will be the maximum number of recovery events that occur in a time interval; moreover, the computation in one iteration only involves vector operations and random number sampling, which can be significantly sped up in other programming languages if necessary.

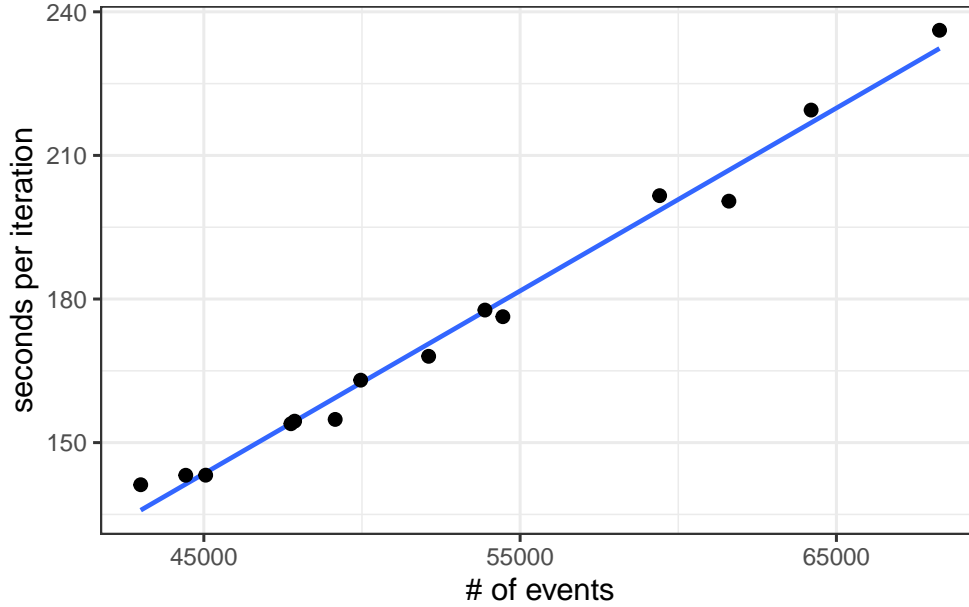


Figure S9: Run time per iteration (in seconds) on **one processor** versus number of observed events in simulations, for population size $N = 500$. Computing time scales linearly with the number of events, and the algorithm can handle data at least at the scale of 10^4 events.

S6 Real Data Experiments

S6.1 Data Pre-processing

All infection events and weekly health statuses of all $N = 103$ individuals are extracted from the weekly surveys. In every survey, study participants were asked if they ever felt ill at all in the past week, if they ever experienced certain symptoms, and, if there were symptoms, when the approximate illness onset time was. We take an “infection” as a positive ILI (influenza-like illness) case, which, following the protocol in Aiello et al. (2016), is defined as a cough plus at least one of the following symptoms: fever or feverishness, chills, or body aches. We further examine each ILI case and only accept one as a positive infection if the individual also indicated that they “felt ill” in the past week, thus eliminating a small number of reoccurring ILI cases for the same participants ⁷. Moreover, since an individual may start

⁷One particular individual had positive ILI cases and felt ill in week 2, 3, and 5, but not in week 4. We therefore treat his/her illness as an extended one, starting in week 2 and lasting till week 5.

exhibiting symptoms at most 3 days *after* getting infected and becoming infectious, for each infection event, we set the “real” infection time as the reported onset time minus a random “delay time” uniformly sampled between 0 and 3 days.

Social link activation and termination events are obtained from the iEpi Bluetooth contact records. Each time two study devices were paired, the iEpi application recorded the unique identifiers of the devices, a timestamp, and a received signal strength indicator (RSSI). Since Bluetooth detection can be activated whenever two devices are within a few meters of each other while the two users may not actually be in contact, we only keep those Bluetooth records with relatively strong signals (high values of RSSIs)⁸. If two consecutive Bluetooth records for one pair of devices are no more than 7.5 minutes apart in time⁹, then the two records are considered to belong to one single continuous contact; a social link between two individuals is activated at the time of the first Bluetooth detection record in a series of consecutive records that belong to a single contact, and the link is terminated at a random time point between 1 and 6 minutes after the last Bluetooth detection of a continuous contact.

The resulting processed data contain 24 infection events in total, with 14 before the spring break week and 10 after, as well as 45,760 social link activation and termination events. The weekly disease status (healthy or ill) of every participant can be acquired from the weekly surveys, so we know, for example, if an individual recovered sometime after day 7 and before day 14, but the exact times of all recoveries are unknown.

S6.2 Maximum Likelihood Estimation

Instead of assuming the knowledge of which infection cases are internal and which are external, we directly estimate all the parameters based on the likelihood function in (22), solving (23) and (24) for the MLEs of β and ξ .

However, the real data are incomplete, with the exact times of all the recoveries unobserved. We resolve this issue using a naive imputation method—for each recovery, an event

⁸The RSSIs range from -109 to 6, and we set the threshold as -90, so only those records with RSSIs larger than -90 are kept.

⁹We choose 7.5 minutes as a threshold instead of 5 minutes to accommodate potential lapses in Bluetooth detection.

time is randomly sampled from a uniform distribution between the time of infection and the earliest time point the individual no longer felt ill (in response to the weekly surveys). Such imputation, of course, is subject to a considerable level of uncertainty, so we randomly generate 10 differently imputed datasets, obtain the MLEs from every dataset, and then report the averages over the 10 runs (see Table S1).

We can see that the MLEs acquired in this manner generally agree with the Bayesian estimates in Section 6.2.

Table S1: MLEs for model parameters using imputed data with all recovery times randomly sampled. The table presents average estimates as well as the standard deviations of estimates over 10 different, randomly imputed datasets. Results generally agree with those acquired using the proposed Bayesian data augmentation inference method.

Parameter	Avg. estimate	Std. deviation
β (internal infection)	0.0676	0.0092
ξ (external infection)	0.00320	1.11×10^{-6}
γ (recovery)	0.236	0.012
α_{SS} (S - S link activation)	0.0530	0.0001
ω_{SS} (S - S link termination)	42.15	0.105
α_{SI} (S - I link activation)	0.0704	0.0028
ω_{SI} (S - I link termination)	52.21	3.83